

# Morphological response to climate-induced flood-event variability in a subarctic river

Linnea Blåfield<sup>1</sup>, Carlos Gonzales-Inca<sup>1</sup>, Petteri Alho<sup>1,2</sup>, Elina Kasvi<sup>1</sup>

<sup>1</sup>Department of Geography and Geology, University of Turku, Finland

<sup>2</sup>Finnish Geospatial Research Institute FGI, National Land Survey of Finland, Espoo, Finland

Correspondence to: Linnea Blåfield, linnea.m.blafield@utu.fi

Formatted: Font: 12 pt

Keywords: Sediment transport hysteresis, Computational modelling, Flood sequencing, Hydroclimatics

## Highlights:

- Sediment transport hysteresis pattern is dependent on the number and volume of flood peak sequences
- Flood-event type significantly impacts the rivers morphological response
- Increase of multi-peaking flood-events, mean temperature, and changing precipitation patterns affects the future river system stability
- Hydrograph shape can be associated to specific preceding climatic conditions

## Abstract

This study examined the effects of climate-induced flood-event variability and peak sequencing on morphological response and sediment transport hysteresis patterns in a subarctic river. We classified 32 years of discharge hydrographs from a subarctic river according to their spring flood hydrograph shapes and peak sequences. These classified flood-event types and their frequencies were statistically analysed against seasonal and annual climatic conditions from the corresponding time periods. Morphodynamic modelling was employed to examine the effects of flood-event hydrograph shape and sequencing on morphological response and sediment transport hysteresis patterns during floods. The findings highlight the critical role that hydrograph shape and sequencing play in influencing river morphology and sediment transport dynamics, as each flood-event type produced distinct sediment transport hysteresis patterns and morphological outcomes. Double-peaking floods resulted in relatively more heterogeneous and complex morphological outcome compared to single-peaking floods. Variance and trend analyses revealed that prevailing climatic conditions significantly influence the hydrograph shapes of spring flood events. Annual mean temperature, total precipitation, and snow accumulation, together with cold season mean temperature, spring rainfall, and May cumulative temperature, had the

Formatted: Font color: Text 1

Formatted: Font color: Text 1, English (United

Formatted: English (United Kingdom)

38 greatest impact on the type of spring flood event observed. Significant increasing trends  
39 were identified in annual and spring mean temperatures, spring rainfall, and the frequency  
40 of rain-on-snow events. This suggests that ongoing climatic shifts are actively modifying the  
41 nature of spring flood events, favouring more complex and variable hydrograph forms.  
42 Consequently, future sediment transport and morphological evolution in subarctic rivers are  
43 likely to become increasingly event-driven, less predictable, and more sensitive to  
44 interannual climatic variability. These changes emphasise the need for adaptive  
45 management strategies that can accommodate the emerging hydrological and  
46 geomorphological dynamics under a changing climate.

47

## 48 1. Introduction

49 Hydrological variability significantly affects riverine sediment fluxes, especially in cold  
50 climate rivers where sediment transport is highly seasonal, occurring predominantly during  
51 spring floods (Syvitski, 2002; Favaro & Lamoureux, 2015; Zhang et al., 2022). Snowmelt-  
52 driven spring floods carry majority of the annual sediment budget and therefore, they define  
53 the timing and volume of sediment transport and ultimately the whole river morphology.  
54 Currently, cold climate rivers are experiencing rapid shifts in hydroclimatic conditions,  
55 influencing the flow-sediment interaction in the river systems (Meriö et al., 2019; Beel et al.,  
56 2021; Li et al., 2021; Zhang et al., 2023; Blåfield et al., 2024a). As hydroclimatic conditions  
57 evolve, the characteristics of flood-events are also changing with implications to the  
58 traditional sediment transport dynamics. For instance, the shift in the snow-to-precipitation  
59 ratio and changes in the timing and intensity of snowmelt have already altered flood  
60 hydrographs i.e., the shape, magnitude, duration, and sediment transport capacity of events  
61 in cold-climate rivers (Wohl et al., 2017; Gohari et al., 2021; Hopwood et al., 2021; Zhang et  
62 al., 2022; Blåfield et al., 2024a; Lintunen et al., 2024). Flood-events are usually classified by  
63 their generating processes (e.g., intense precipitation, snowmelt, rain-on-snow, ice jamming,  
64 dam break etc.), with less emphasis on the event type and sequences itself. Previous studies  
65 (Viglione et al., 2010; Fischer et al., 2019; Gohari et al., 2022), however, have reported that  
66 ongoing regime shifts have altered flood-event shapes. Over the past century, multi-peaking  
67 floods have become more common, not only in central Europe, but also in high-latitude  
68 regions.

69

70 In multi-peaking floods, the order and duration of different peaks significantly affects the  
71 sediment transport volume and the pattern of sediment transport hysteresis because the  
72 flow conditions control when, how much, and what type of sediment is mobilised, reworked,  
73 or deposited within the river system (Mao, 2018). Therefore, understanding the contribution  
74 of flood-event sequences to sediment transport is crucial for predicting the impact of climate  
75 change on fluvial sediment dynamics and the morphological response of river systems (Mao,  
76 2012; Karimaee Tabarestani & Zarrati, 2015). This is particularly important in cold-climate  
77 rivers, which have historically experienced a single major snowmelt-driven flood and low  
78 sediment loads. However, due to hydroclimatic regime shifts, altered fluvial dynamics and  
79 possible permafrost or glacier melt, these regions are increasingly becoming hotspots for  
80 elevated sediment transport (Syvitski et al., 2002; Li et al. 2021; Zhang et al., 2022). Recent  
81 studies indicate that migration rates of large, sinuous rivers in the Arctic permafrost region

Formatted: Font color: Text 1, English (United

Formatted: English (United Kingdom)

Formatted: Font color: Text 1, English (United

82 have slowed by 20% during the past 50 years due to decreased fluvial energy and increased  
83 bank shrubification (Ielpi et al., 2023). Contrasting findings have been made on the Tibetan  
84 Plateau where migration rates have increased by 34% due to increased discharge volumes  
85 and river bank destabilisation caused by permafrost melt (Sha et al., 2025). In boreal-  
86 subarctic regions, where the focus of this study is, the fluvial activity and extreme discharge  
87 events outside the spring flood season have increased while spring flood peaks have  
88 decreased significantly (Korhonen & Kuusisto, 2010; Lintunen et al., 2024). The increased  
89 fluvial activity outside traditional flood season is caused by increasing number of extreme  
90 rainfall events (Nikulin et al., 2011) which are intensifying bank erosion and sediment  
91 transport (Kärkkäinen & Lotsari, 2022). However, the annual total volume of water has not  
92 yet changed (Lintunen et al., 2024). All these findings suggest that climate change has  
93 diverse impacts on fluvial dynamics across the high-latitude region, and therefore more  
94 focus should be paid sediment transport dynamics and the hysteresis pattern under evolving  
95 discharge conditions. Understanding these processes is essential because sediment  
96 transport not only shapes river morphology but also governs aquatic habitats, influences  
97 nutrient fluxes, and affects infrastructure stability.

98

99 One effective way to evaluate the sediment transport process and morphological response  
100 of the river channel is through analysis of sediment transport hysteresis patterns, which  
101 reflect the sediment transport affected by riverbed structure, sediment composition and  
102 availability at different stages of the flow hydrograph (Williams, 1989; Reesink & Bridge,  
103 2011; Gunsolus & Binns, 2017). In cold climate rivers various types of sediment transport  
104 hysteresis have been observed due to highly seasonal and varying sediment availability  
105 between catchments (Vatne et al., 2008; Kociuba, 2021; Wenng et al., 2021; Zhang et al.,  
106 2021; Liébault et al., 2022). Yet, measuring bedload and hysteresis in natural rivers during  
107 high flows remains challenging and is prone to biases. As a result, long time series of  
108 bedload transport and hysteresis are scarce worldwide (Mao, 2018; Zhang et al., 2023).  
109 Thus, we rely on laboratory experiments, computational modelling, and field measurements  
110 of suspended load when evaluating and measuring the current, and predicting the future  
111 sediment fluxes and morphodynamic response of the river channels.

112

113 The ability to evaluate and predict the effects of climate change on sediment transport rates  
114 and morphological response is essential not only for understanding fluvial morphodynamics,  
115 such as channel stability and sediment connectivity but also for a wide range of river  
116 engineering and management applications (Mao, 2018; Gupta et al., 2022; Najafi et al.,  
117 2021). Therefore, this study aims to: i) Analyse and classify the variation in flood-event  
118 hydrographs over the past 32-years in a subarctic river, ii) Link the flood-events to seasonal  
119 and annual climate conditions, and iii) Evaluate the channels morphological response  
120 distinctive to each flood-event type utilising morphodynamic modelling and sediment  
121 transport hysteresis analysis. We expect to detect linkages between the flood-event  
122 hydrograph shape and climatic conditions as well as diverse patterns of morphological  
123 response and sediment transport hysteresis. The study was conducted on a river reach in  
124 Finland, located at 70° North latitude. Despite its high latitude, Finland has a relatively mild  
125 climate compared to other regions at similar latitudes, such as Siberia, northern Canada,

126 and Alaska, largely due to the warming influence of the Gulf Stream and the North Atlantic  
127 Drift. As a result, Finland is mostly free of permafrost (Luoto et al., 2004), although small  
128 areas of permafrost exist in the form of palsas. These palsas are primarily found in  
129 north-western Finland (Seppälä, 1997; Gislén et al., 2017; Verdonen et al., 2023).  
130 Nevertheless, Finland experiences seasonally frozen ground for periods ranging from four  
131 (South) to eight (North) months each year (Rimali, 2019).

132

133 **2. Study area**

134 The meandering and unregulated Pulmanki River locates in northern Finland (Fig. 1A) The  
135 river is a tributary to Tana River which flows into the Arctic Ocean on Norwegian side of the  
136 border (Fig. 1A). The river is divided into two separate sections by the Lake Pulmankijärvi  
137 (Fig. 1B). The area of interest in this study is a 6-kilometre-long reach on the upper course  
138 of the Pulmanki River approximately 13 meters above the mean sea level (a.m.s.l) (Fig. 1B).  
139 This reach consists of 13 meander bends with a reach sinuosity of 2.4. The bankfull width  
140 of the river varies between 60 to 100 metres, depending on the valley confinement. The river  
141 flows through glaciolacustrine and glacio-fluvial sediments deposited on the fjord bottom  
142 after the final wasting of Fennoscandian ice sheet (Mansikkaniemi, 1967; Hirvas et al., 1988;  
143 Johansson et al., 2007). The D50 value of the channel bed material ranges from 0.1 mm to  
144 4 mm and a sandy bedload (D50 0.43 mm) dominates the sediment transport. The amount  
145 of suspended material is minimal (0-180 mg/L), even during the spring flood (Lotsari et al.,  
146 2020). The bed morphology is typical for sand bed rivers and consists of dunes, ripples,  
147 pools, and riffles, the bed is unvegetated and mobile through the year. The channel is frozen  
148 from October to May, and the seasonal discharge ranges from 0.5 to 100 m<sup>3</sup>/s. A spring  
149 flood generated by the snowmelt occurs annually in late-May or early June. Lower discharge  
150 peaks are associated with precipitation events during July, August and September. The river  
151 belongs to subarctic-nival hydrological regime (Lininger and Wohl, 2009) and to Köppen  
152 climate class: "Cold, without dry season, but with cold summer" as the area is affected by  
153 the great Asian continent and both the Atlantic Ocean and the Gulf Stream. Based on the  
154 Nordic permafrost model by Gislén et al., (2017) majority of the catchment is permafrost  
155 free (Fig. 1C). The south-western corner has 10-50 % probability of sporadic permafrost  
156 according to the model results based on land cover, snow accumulation and temperature  
157 data. However, no confirmed field observations of sporadic permafrost from the area exist,  
158 and therefore we consider this catchment and river system as non-permafrost river.

159

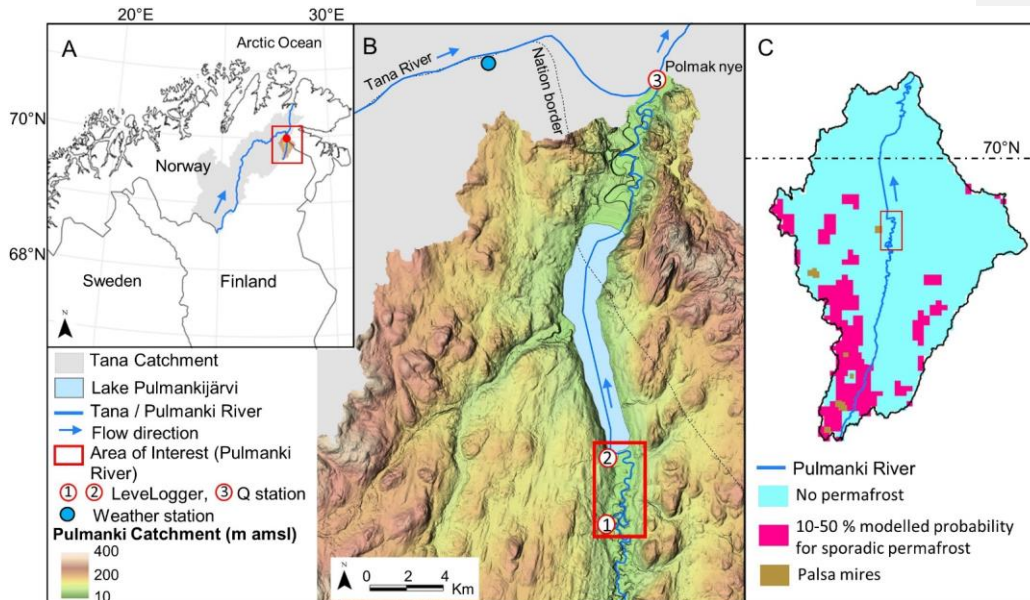


Figure 1. Area of interest. A) The study area's location in the Northern most Finland. B) Model area is marked with rectangle, and the locations of LeveLogger sensors (LL), discharge (Q), and weather station with circular markers. C) The probability of sporadic permafrost within the catchment based on the Nordic permafrost model by Gissnäs et al., 2017. Pulmanki catchment 2x2 m DEM by National Land Survey of Finland.

### 3. Data & Methods

Discharge hydrographs of the years 1992-2023 were analysed and classified to recognise variability in spring flood-event shapes. The most typical flood-event of each hydrograph type was selected for morphodynamic modelling to evaluate the channels morphodynamic response and sediment transport dynamics. The flood-events extracted from the classified hydrographs were linked with climate data from equivalent time period to examine possible connections between climate and flood-event shapes. Mann-Kendall trend test was run on the hydroclimatic variables to detect possible trends in the time-series. Continuous discharge and water level monitoring has been conducted in Pulmanki River since 2008 during open water season (May-September). The Pulmanki River discharge time-series was complemented with Polmak discharge station data from Tana River (Fig. 1) to cover the whole 32-year time period. Sediment and bedload transport samples were collected during the spring and autumn field campaigns in 2019 from various discharge conditions.

Formatted: Indent: Left: 0 cm

### 184 3.1 Hydrograph measurements and generation

185 Hydrographs of open water season were generated utilising a combination of data sources.  
186 For the years 2008-2023, rating curves based on a combination of field data were generated:  
187 water pressure sensor data (Levellogger 5, Solinst), water level data measured with Virtual  
188 Reference Station-Global Navigation Satellite System (VRS-GNSS), and discharge data  
189 measured with Acoustic Doppler Current Profiler (ADCP M9, Sontek). Each year, the water  
190 pressure sensors were placed into the upper Pulmanki River after ice-breakup in spring and  
191 picked up before winter (see locations in Fig 1). This way the sensors covered the whole  
192 open water season and seasonal variations of water pressure, water level and discharge  
193 with 15 minute intervals. The location of the sensors was identical each year. To compensate  
194 atmospheric influence on water pressure, an air pressure sensor data from Solinst  
195 Barologger was subtracted from the water pressure readings. During field campaigns in May  
196 and September water level and discharge were measured daily from the LeveLogger  
197 locations for creating rating curves between LeveLogger pressure, water level (WL) and  
198 discharge (Q). Based on the rating curves, a 3<sup>rd</sup> order polynomial function was selected for  
199 calculating annual hydrographs of open water seasons (Figure 2A).

200

201 For the years 1992-2007, openly available daily discharge data from Polmak measurement  
202 station, maintained by the Norwegian Water Resources and Energy Directorate (NVE) was  
203 used. The station is located in the main channel of Tana River at the spot where Pulmanki  
204 River discharges into Tana (see Fig. 1, Q station number 3), and has been operating since  
205 November 1991. The discharge for Pulmanki River was derived from the Polmak station data  
206 using rating curve and 3<sup>rd</sup> order polynomial function between the Polmak station discharge  
207 (Q) and Pulmanki River Q of 2008-2023 derived from the LeveLoggers (Figure 2B). Note  
208 that the discharge of the Tana River continues to rise even as the discharge of the Pulmanki  
209 River decreases, owing to the fact that the Tana River drains a catchment area 20 times  
210 larger than that of the Pulmanki River. The Pulmanki River catchment (a sub-catchment of  
211 the Tana) is situated approximately 200 km downstream from the Tana River headwaters  
212 and lies in much lower terrain (with a maximum elevation of 400 m above sea level),  
213 compared to the Tana catchment, which includes areas reaching up to 1,100 m above sea  
214 level. This results in a delay in snowmelt, causing peak runoff in the Tana River to occur later  
215 than in the Pulmanki catchment. The final hydrographs of Pulmanki river are based on these  
216 two equations and data sources. The hydrographs were validated against ADCP discharge  
217 measurements from Pulmanki River main channel. These measurements were excluded  
218 from the rating curve creation. See the details of error metrics in Table 1.

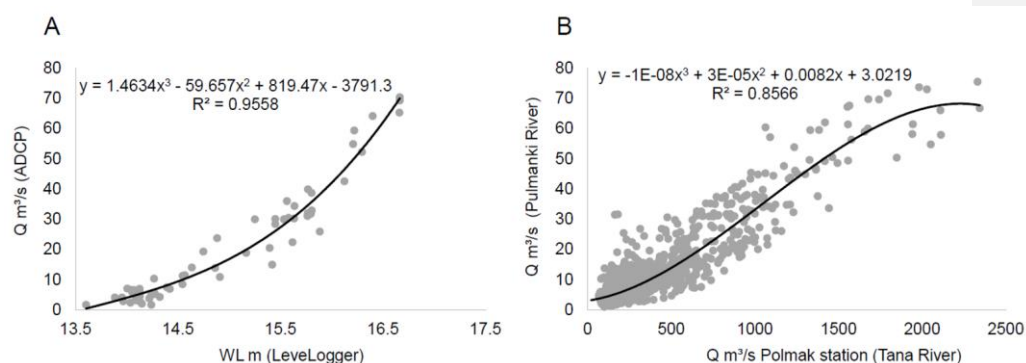


Figure 2. Rating curves for Pulmanki River hydrographs. A) Regression curve of discharge measurements (Q m³/s ADCP) and LeveLogger water level (WL) in Pulmanki River 2008-2023. This polynomial function A was used to calculate hydrographs for years 2008-2023 B) Regression curve showing the relationship between the discharge in Pulmanki (Q m³/s calculated based on regression curve A) and Polmak (Q m³/s measured, national gauging station) during 2008-2023. This polynomial function B was used for calculating Pulmanki River discharge for years 1992-2007.

Table 1. Error metrics of the final hydrographs derived from two different data sources: LeveLogger discharge data and Polmak Station discharge data. MAE = Mean Absolute Error, SDE = Standard Deviation of Error, r = Correlation Coefficient, n = Number of samples.

Pulmanki River Q Derived from:	Min. Error (m³/s)	Max. Error (m³/s)	Mean Error (m³/s)	MAE (m³/s)	SDE (m³/s)	r	R²	n
LeveLogger	-9.59	10.73	-0.24	2.92	3.74	0.94	0.89	152
Polmak Station	-51.48	20.34	-0.39	2.59	4.65	0.89	0.80	1804

### 3.2. Hydrograph classification

The hydrographs were classified into distinct flood-event types based on the peak shape in Python program using the SciPy Scientific Python (SciPy) library. A threshold value of 23.46 m³/s (75<sup>th</sup> percentile, p75 discharge) for flooding was set to classify significant spring flood-events. A sensitivity analysis on peak-finding thresholds was conducted using the 50th, 60th, 70th, 80th, and 90th percentiles. Threshold values at the 70th and 80th percentiles were found to capture the majority of relevant spring flood events, and consequently, the 75th percentile (p75) was selected for this study. The commonly used threshold of the 90th percentile (Q > 58 m³/s in this case) restricted the dataset too severely, with the algorithm failing to detect spring floods in certain years, particularly those with low peak discharges. Furthermore, using the p90 value resulted in hydrographs that included only the very peak of the flood event, without capturing the rising and falling limbs of the hydrograph, which are crucial for evaluating sediment dynamics and flow–sediment interactions. Thresholds below



the 70<sup>th</sup> percentile included peaks outside of spring flood season, and thus these thresholds were not ideal for this study. The definition for high and low flood-event was set to be either above or below the mean flood discharge of 40 m<sup>3</sup>/s, respectively.

The event classification was done by estimating different flood peak features such as peak timing, prominence, peak height, and event duration. First, a Savitzky-Golay smoothing filter was applied to the dataset to reduce noise and enhance the detectability of flood peaks. This was accomplished using the `Savgol_filter` function from the `scipy.signal` module, with a window size of 11 and a polynomial order of 3 to preserve relevant hydrograph features. Peak shapes within the smoothed data were identified and classified into distinct flood-events using the `find_peaks` function from the `scipy.signal` module. The following parameters and minimum values were found to most effectively identify peak events: the minimum discharge threshold for a flood event, defined as the 75th percentile (p75 Q), a minimum hydrograph width of one day, measured from the start of the rising limb to the end of the recession limb, and a minimum prominence of 2 m<sup>3</sup>/s, indicating how much the peak stands out from the surrounding baseline.

Four different event types were detected: A) High one-peak ( $Q > 40$  m<sup>3</sup>/s), B) Low one-peak ( $Q < 40$  m<sup>3</sup>/s), C) Two separate peaks ( $Q > p75$ ,  $Q < p75$ ,  $Q > p75$ ), and D) Wavy peak (two  $Q > p75$  peaks) (Figure 3A-D). For modelling purposes, the most typical event of each type was selected (red solid line in Fig. 3A-D). The precipitation-driven discharge peaks in July, August and September were left out of the analysis as none of them exceed the flood threshold discharge of p75. In addition, previous studies indicate that the majority of high-latitude rivers transport most of their annual sediment load during the main flood event, namely the spring flood (Syvitski, 2002; Zhang et al., 2022; Blåfield et al., 2024b). Therefore, the focus of this study was placed solely on spring flood peaks. In this region, spring flood peaks are driven by climatic factors such as rising temperatures and rainfall, which induce snowmelt, increase runoff, and lead to the break-up of river ice cover.

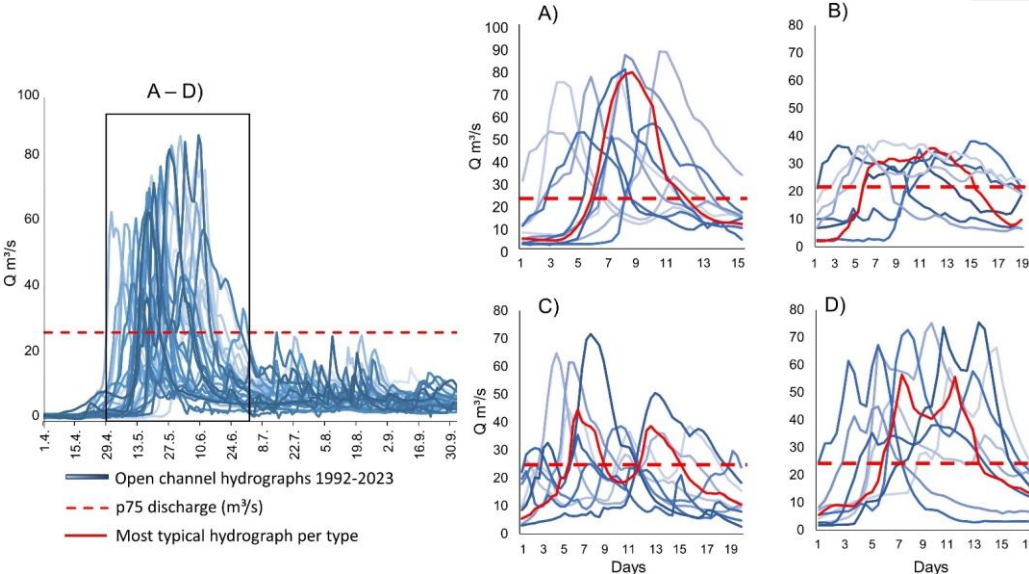




Figure 3. All the generated hydrographs of years 1992-2023. The classification led to four distinct flood-event shapes: A) High one-peak flood, B) Low one-peak flood, C) Flood with two separate peaks, and D) Flood with a wavy peak. The solid red hydrograph is the most typical flood-event of each shape which was thus used in the morphodynamic model. Red dashed line is the 75th percentile threshold discharge for spring flood.

### 3.3. Hydroclimatic data and statistical analysis

Climate data from the Nuorgam weather station (see location in Fig. 1B), 11 metres above the mean sea level and 17 kilometres North from the Pulmanki River study area, was downloaded from the Finnish Meteorological Institutes open data service. Daily Total, Min, Mean and Max temperature, precipitation, and snow depth data of years 1991-2023 were selected for the variance and trend analysis as these variables are closely related to the hydrological properties of rivers (Veijalainen et al., 2010; Irannezhad et al., 2022). Annual Min, Mean, Max and Total values were derived from the daily data and used in the trend analysis (Fig. 4). In addition, duration of snow cover, number of precipitation-days, and occurrence of extreme snow/precipitation events (95<sup>th</sup> percentile) were derived for the trend analysis. For detailed analysis of springtime trends, the corresponding measures were derived for March, April, and May as well. Only one weather station was included in the analysis as other stations are located 50-100 kilometres away with over 100-meter elevation difference to the area of interest. The year 1991 was included in the climate time-series as the analysis was conducted on hydrological years instead of calendar years.

The Mann-Kendall (M-K) trend test was carried out on all climate variables with  $\alpha = 0.05$  significance level to identify statistically significant monotonic trends. In addition to climate variables, the MK-trend test was run on the classified flood hydrographs to examine trends in the occurrence-interval, timing, volume, and duration of each flood-event hydrograph type. Possible serial correlations were removed by using Hamed & Rao (1998) M-K modification which is explained in detail in e.g., Daneshvar Vousoughi et al., (2013) and in Jhajharia et al., (2014). The effect of outliers on the trend was removed by using a non-parametric linear regression Sen's slope estimator (Sen, 1968). Analysis of Variance (ANOVA) with  $\alpha = 0.05$  significance level was run to identify possible significant differences between the means of the variables, i.e. whether the annual/cold-season/spring or May weather conditions differ significantly across the four spring flood-event type.

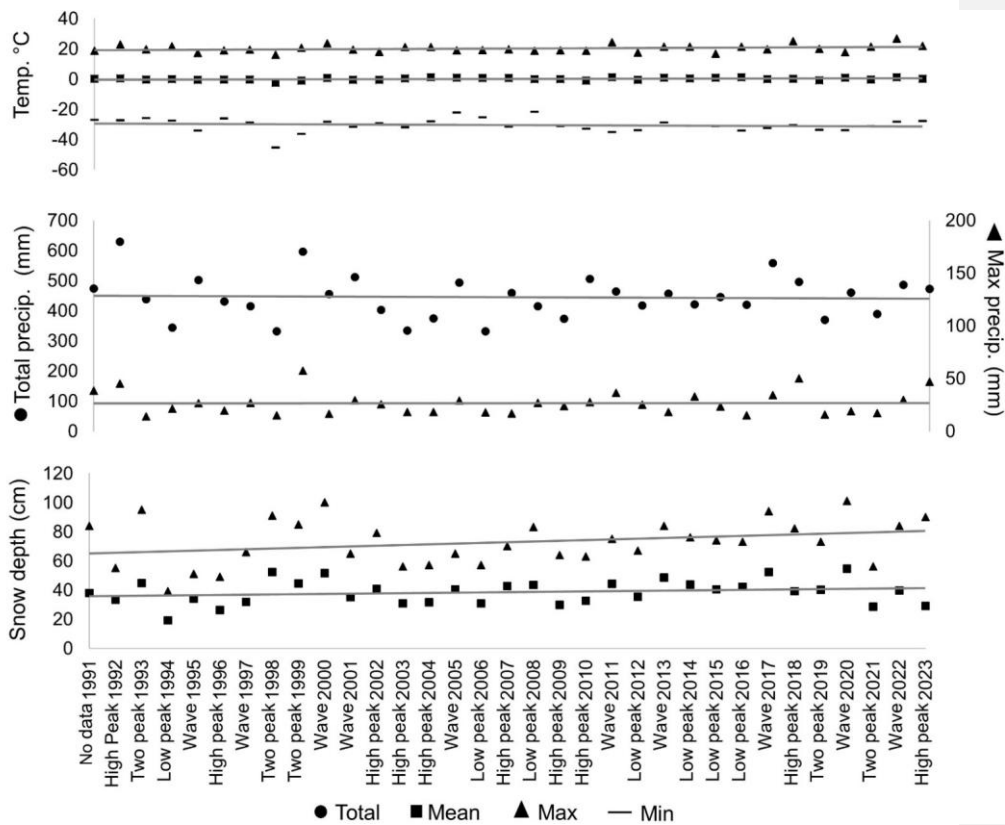


Figure 4. The annual climate time-series of the 32-year time period derived from the daily data. The corresponding flood-event types are marked on the x-axis.

### 3.4. Sediment and bedload sampling

Both grab samples with Van Veen sediment sampler, and bedload samples with Helley-Smith sampler were collected from the riverbed in 2019. A total of 70 grab samples (ca. 500 g) and 24 bedload transport samples were collected during various discharges from the area of interest. Grab samples were collected across the entire 6-kilometre reach during a single autumn field campaign under low discharge ( $4.2 \text{ m}^3/\text{s}$ ) conditions. Samples were taken from the channel bed at left and right bank of each meander inlet, apex and outlet. Bedload transport samples were obtained during both, spring and autumn campaigns, under varying discharge levels ( $7.5 \text{ m}^3/\text{s}$ ,  $56 \text{ m}^3/\text{s}$ , and  $4.2 \text{ m}^3/\text{s}$ ). Twelve bedload transport samples were collected per campaign, each with a sampling duration of six minutes. The samples were dry sieved using half-phi intervals and the amount of material in each sieve was weighted. Sample statistics were calculated in GRADISTAT-program (Blott & Pye, 2010) using the Method of Moments which is based on a logarithmic distribution of sample phi sizes. GRADISTAT utilises its own scale with only four classes (Silt,  $0.002\text{--}0.063 \text{ mm}$ , Sand,

0.063–2 mm, Gravel, 2–64 mm and Boulders 64–2048 mm). The results of sediment and bedload sampling were utilised in the morphodynamic model as multiple sediment fractions, spatially varying Manning's Roughness parameter, and for calibrating and validating the sediment transport rates (see details in Blåfield et al., 2024b).

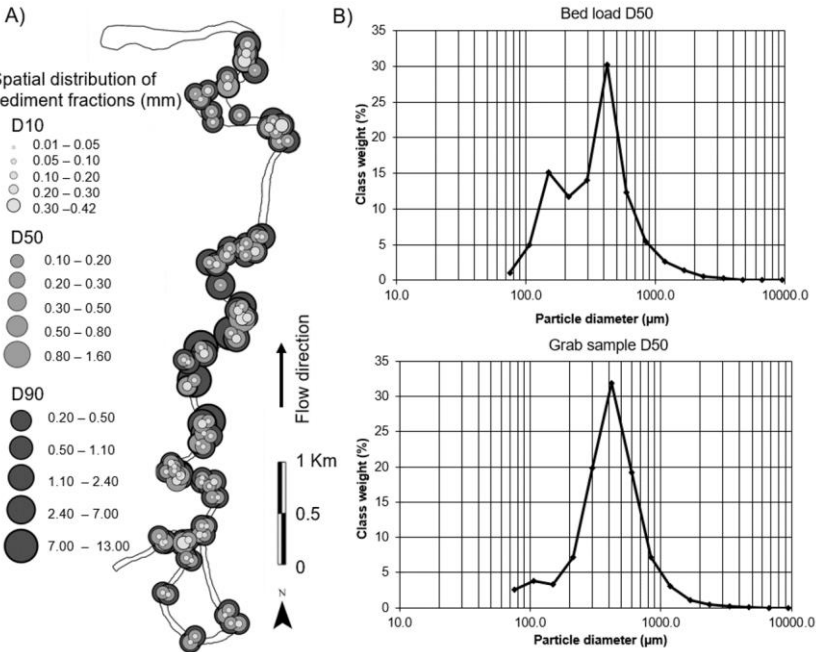


Figure 5. A) Spatial distribution of sediment fractions D10, D50 and D90 based on the collected field samples. B) D50 particle diameter distribution of all the collected bedload and grab samples in micrometres.

### 3.4 Morphodynamic modelling

The authors have previously presented and validated the model used in this study (Blåfield et al., 2024b). In this study, four distinct flood-event hydrographs (A-D in Table 2.) were simulated using the same initial channel geometry and sediment composition. A depth-averaged morphodynamic model with curvilinear, unstructured grid of 2x2 meter cell size was built utilizing FLOW 2D-module of Delft3D software. The model geometry was based on a digital elevation model derived from Structure-from-Motion (SfM). Specific details of the SfM creation can be found in Blåfield et al., (2024b), and general from Micheletti et al., (2013), and Dietrich et al., (2017). Multiple sediment fractions and spatially varying Manning's Roughness based on the grab sediment samples from the field were used, as these additions have been shown to significantly improve predicted morphodynamics (Kasvi et al., 2014). Each simulation featured hourly varying discharge conditions to evaluate sediment transport dynamics, sediment transport hysteresis patterns, and morphological responses to the shape and sequencing of the simulated hydrographs. The model time-step

was set to 0.05 minutes, with both spin-up and output intervals set at 720 minutes. Morphology, source and sink terms, and total sediment transport were updated at each time step. The model solved morphology independently based on the source and sink terms of van Rijn (1993) approach. Transport boundary conditions, i.e., sediment feeding into the model, were solved using the Neumann law and updated at each time-step. This allowed the model to dynamically adjust the sediment supply and concentration at the inflow to match the internal model conditions, thereby minimising accretion near the model boundaries. Subsequently, sediment transport hysteresis and geomorphic activity for each flood-event type were calculated from the source and sink terms, as well as from the modelled total volume of sediment mobilised within the inundated area. The default scheme for dry-cell erosion of banks was applied without further adjustment, as the focus of the study was on longitudinal sediment transport and vertical changes to the channel bed. Detailed parametrisation, as well as the model's calibration and validation are provided in Blåfield et al., (2024b).

Delft3D is unable to simulate ice-covered flows or the effects of freeze–thaw processes on bank erosion. These limitations, together with the absence of vertical flow representation in the two-dimensional simulation, introduce simplifications into the modelling of flow dynamics and sediment transport. The use of user-defined parameters further contributes to uncertainty, particularly in the spatial and temporal patterns of erosion, transport, and deposition. The van Rijn (1993) approach is sensitive to user-defined parameters such as sediment fraction, composition, and associated threshold conditions (Pinto et al., 2006). However, Kasvi et al. (2014) demonstrated that the van Rijn formulation performs more reliably when applied with spatially variable, field-based sediment fractions and Manning's roughness coefficients rather than uniform values. While the van Rijn transport formula typically produces lower transport rates than other formulations (Schuurman et al., 2013; Kasvi et al., 2014), it remains widely regarded as the most physically based and reliable method (Pinto et al., 2006; Kasvi et al., 2014). The user-defined parametrisation used in the present study is detailed in Blåfield et al. (2024b). Spatial variability in sediment grain size and Manning's roughness, alongside the inclusion of medium transverse bed slope effects, were identified as key parameters influencing sediment load predictions and morphological change (Nicholas, 2013; Kasvi et al., 2014), and were prioritised for refinement during simulation.

Table 2. The details of each model run. The flow conditions of flood-events A-D are based on the hydrograph classification in section 3.2. The morphological parameters are based on the sediment and bedload sampling from the field.

Event	Duration (days)	Peak Q m <sup>3</sup> /s	Total Q Volume m <sup>3</sup>	Sediment Supply	Morphology	Sediment composition
A	7	80	29 868 586	Feeding	Sand bed	Sand, Gravel
B	13	35	34 851 505	Feeding	Sand bed	Sand, Gravel
C	14	48	26 2383 45	Feeding	Sand bed	Sand, Gravel
D	9	60	31 20 1609	Feeding	Sand bed	Sand, Gravel

381  
382  
383  
384  
385

386 **4. Results**

387

388 **4.1 Hydroclimatic conditions and flood-event type variability**

389 The variance analysis of flood events of types A–D and the prevailing climatic conditions  
390 indicated that the climatic conditions of the preceding hydrological year were the most  
391 significant of the tested variables influencing the type of spring flood event (Table 3). Other  
392 significant factors influencing the flood-event type included the cold season (October–May)  
393 mean temperature, spring rainfall (March–May), and May warmth, expressed as the  
394 cumulative temperature sum in May (Table 3). In addition to climatic conditions, the timing  
395 of peak discharge varied significantly between event types. The number of snow cover days  
396 in May demonstrated a trend approaching statistical significance (Table 3). By contrast,  
397 rainfall during the cold season, May rainfall, and the spring mean temperature did not exhibit  
398 significant differences between flood-event types (Table 3).

399 Flood events of Type A were typically associated with high annual snow accumulation, low  
400 annual temperatures, and rapid warming in May, resulting in a low number of snow cover  
401 days during May (Fig. 6). These events also experienced high annual precipitation but low  
402 spring rainfall (Fig. 6). Thus, flood events of Type A can be characterised as occurring in  
403 cold, snow-rich years, where rapid warming in May leads to sharp and high flood  
404 hydrographs. Flood events of Type B were associated with the warmest cold season mean  
405 temperatures, along with moderate spring rainfall, snow accumulation, and cumulative May  
406 temperatures (Fig. 6). These conditions suggest that snowmelt may begin during the cold  
407 season and continue through spring, resulting in reduced energy availability during the main  
408 melt period in May. Flood events of Type C were linked to the lowest annual precipitation,  
409 the lowest cold season temperatures, and the coldest May temperatures (Fig. 6). However,  
410 these events also exhibited the highest snow accumulation during spring. Overall, Type C  
411 floods reflect dry, mixed, or transitional climatic conditions, in which a particularly cold winter  
412 and spring lead to delayed snowmelt. This delayed melt, when combined with May rainfall  
413 and variable temperatures, may result in two distinct melt peaks. Flood events of Type D  
414 were characterised by high annual and spring snow accumulation, alongside the warmest  
415 annual and cold season mean temperatures, but relatively low temperatures in May, leading  
416 to a prolonged persistence of snow cover during May. These events also experienced high  
417 annual precipitation and considerable variation in spring rainfall. Consequently, this flood  
418 type typically occurs following a warm and wet year, when May is cold and experiences  
419 highly variable rainfall, resulting in non-uniform snowmelt and the development of wavy  
420 hydrographs.

421 Table 3. Results of one-way ANOVA test on the main variables with  $\alpha = 0.05$  significance  
422 level. Statistically significant p-values are bolded. T = Temperature, P = Precipitation, Cold  
423 season = October-May, Spring = March, April, May.

424  
425  
426  
427  
428  
429  
430

Formatted: Indent: Left: 0 cm

Variable	F-statistics	p-Value
Annual mean T	3.73	<b>0.022</b>
Annual snow sum	7.73	<b>0.006</b>
Annual total P	4.00	<b>0.017</b>
Cold season mean T	3.38	<b>0.032</b>
Cold season Rainfall	2.26	0.104
Spring mean T	1.78	0.174
Spring snow sum	1.93	0.103
Spring rainfall	3.13	<b>0.050</b>
May cumulative T	3.41	<b>0.032</b>
May n. of snow cover days	2.36	0.083
May Rainfall	0.97	0.420
Peak Q timing	3.28	<b>0.035</b>

431

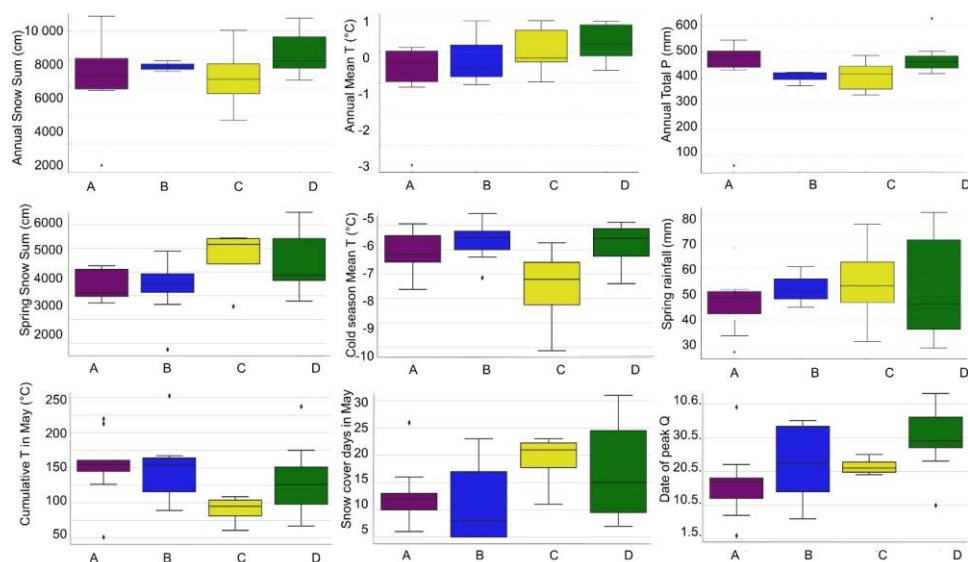


Figure 6. Statistically significant differences between the variable means illustrated in the boxplots, showing the distribution, median, and variation of climate variables associated with each flood-event type. Two borderline variables close to significance (May snow cover days and spring snow sum) were plotted as well.

The wavy (D) and high one-peak (A) events appeared the most frequently, both occurring 10 times within the 32-year time-series. The wavy events of type D had an average duration of 9 days whereas high one-peak event of type A lasted 7 days on average. Low one-peak events of type B occurred 7 times and had the longest average duration of 13 days. Finally, the two-peak events of type C were the least frequent type with only five occurrences lasting 14 days on average. No significant trends were observed in re-occurrence-interval, duration, volume, or timing of any of the flood-event types within the 32-year time-series (Fig. 7). Trend analysis on the climate variables indicate that in snow-related variables (mean, maximum, and extreme snow), all annual trends (square marker) were positive with statistically significant increase. The max snow amount had statistically significant trend also in spring (March-May, circle marker). The number of snow days, however, showed a non-significant weakly negative trend (Fig. 7). Temperature trends were mostly positive, with statistically significant increases in both annual and spring mean temperature (Fig. 7). Spring-time max temperature had significant increasing trend indicating that especially springs have gotten warmer over the time-series. Minimum temperature showed non-significant trend in annual and spring-time data. Precipitation-related trends were more variable. Mean and max precipitation exhibited mostly negative non-significant trends or no trend at all, while the annual extreme precipitation (95<sup>th</sup> percentile) showed significant decreasing trend (Fig. 7). Even though the spring-time precipitation did not indicate significant trends in volume, the number of precipitation days had significant increasing trend.



Overall, the results suggest that while the frequency and characteristics of individual flood-event types have remained relatively stable over the 32-year period, underlying climatic drivers have undergone notable changes. In particular, the increase in snow accumulation and rising spring temperatures point toward a shift in the timing and dynamics of snowmelt, even if not yet reflected in observable flood trends. The significant rise in the number of precipitation days during spring, despite no clear trend in total precipitation volume, may also contribute to more fragmented or prolonged runoff events, potentially supporting the occurrence of events of type B and D.

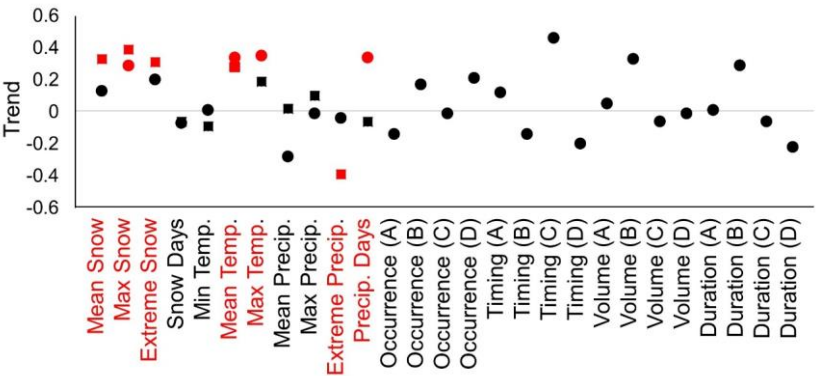


Figure 7. The M-K-trend test results of the climate-related variables during the 32-year study period. Red markers indicate statistically significant trends and black markers non-significant. Square markers represented annual trends, while circles represent seasonal trends in spring (March-May).

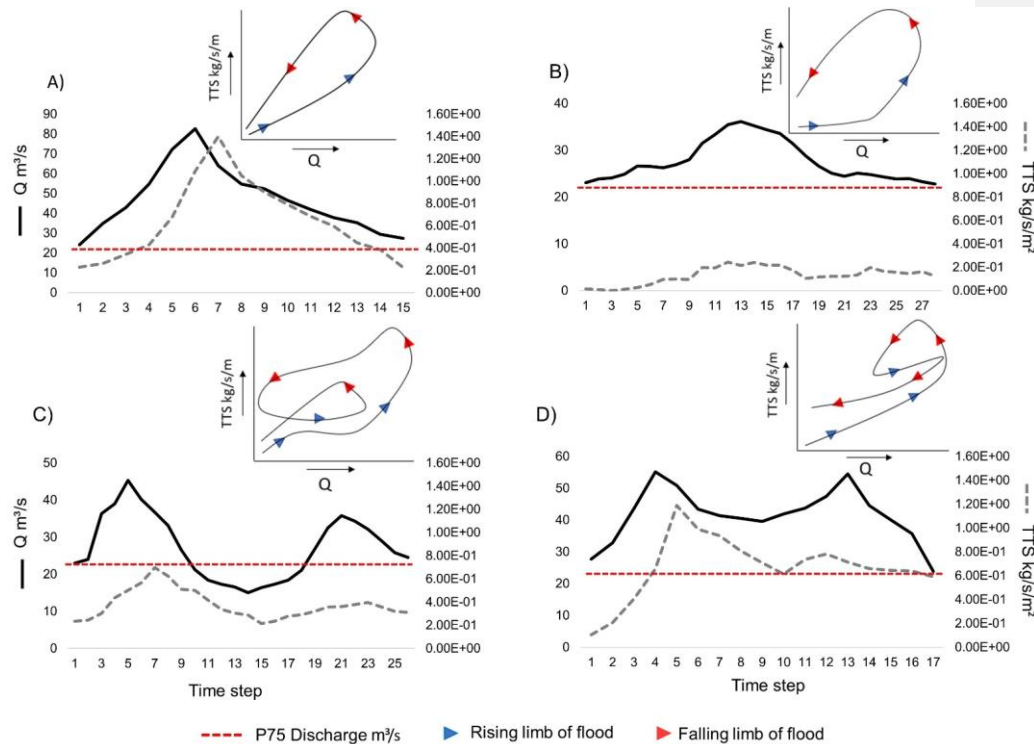
#### 4.2 Morphological response to sediment transport hysteresis

The modelled results suggest that hydrograph shape may have a significant influence on morphological response and sediment transport hysteresis. Both the total transported sediment ~~(TTS, calculated across the entire model area) TTS~~ and the type of sediment transport hysteresis appeared to vary across the modelled events. The wavy event (Type D) was associated with the largest volume of TTS, with the first peak contributing approximately 59% and the second peak 41% of the event's TTS. Thus, the transport rate during the first peak was about 28% higher than during the second peak. In the flood event characterised by two separate peaks (Type C), the first peak contributed 63% and the second 37% of the total TTS. Consequently, the transport rate during the second peak was approximately 42% lower than during the first. The TTS of event C was around 17% lower than that of event D. The high one-peak event (Type A) yielded a TTS volume approximately 4% lower than event D and about 11% higher than that of event C. In contrast, the low one-peak event (Type B) exhibited a TTS volume about 30% lower than that of the high one-peak event (Type A), and approximately 20–32% lower than the double-peaking events C and D, respectively.

All events predominantly exhibited counterclockwise sediment transport hysteresis, where the transport peak occurred after the peak discharge (Fig. 8A–D), suggesting that sediment transport lagged behind changes in discharge and flow conditions. However, the modelled

Formatted: Font color: Text 1, English (United

489 sediment transport hysteresis loops appeared to vary in complexity and shape depending  
 490 on the flood-event type.  
 491 The single-peak events (Types A and B) displayed relatively simple counterclockwise loop-  
 492 shaped hysteresis, with sediment transport following the peak discharge (Fig. 8A–B). Event  
 493 C appeared to exhibit a more complex hysteresis pattern, including multiple  
 494 counterclockwise loops, which may indicate that sediment mobilised during the first peak  
 495 was partially deposited between the peaks, as the second peak showed significantly lower  
 496 TTS (Fig. 8C). In the wavy event (Type D), the first peak exhibited counterclockwise  
 497 hysteresis, whereas sediment transport during the second peak appeared to precede the  
 498 second discharge peak, resulting in clockwise hysteresis (Fig. 8D). This complexity may  
 499 reflect variability in sediment mobilisation processes and sediment availability.  
 500 Across all events, higher TTS values were observed during the falling limb compared to the  
 501 rising limb at corresponding discharge values, suggesting that sediment transport was not  
 502 directly proportional to discharge (Fig. 8A–D). This discrepancy highlights the potential  
 503 influence of delayed and progressive sediment mobilisation, as well as the lagged  
 504 morphological response of bedforms. These findings imply that flood-event shape may have  
 505 a considerable influence on sediment transport hysteresis and, consequently, on riverbed  
 506 morphological development.



507 Figure 8. The modelled flood-event hydrographs and sediment load at each timestep. On  
 508 the upper right corner of each graph is the sediment transport hysteresis of the event type.  
 509 The blue arrows indicate rising limb and red arrows falling limb of the flood. The red dashed  
 510

line shows the threshold p90 discharge. A) High one-peak event and sharp counterclockwise sediment transport hysteresis. B) Low one-peak event and wide counterclockwise sediment transport hysteresis. C) Event with two separate peaks and counterclockwise sediment transport hysteresis with a loop. D) Wavy type event and hysteresis loop with counterclockwise and clockwise directions.

Each modelled event appeared to demonstrate different patterns of morphological response (Fig. 9A–D), influenced by variations in sediment transport hysteresis, stream power, and flow velocity. Event A produced the second highest total volume of mobilised sediment and geomorphic activity (Fig. 9A). Based on the model, this event appeared to experience the most extensive erosion throughout the reach, with deposition areas remaining relatively localised. The highest stream power values were modelled in this event, exceeding  $24 \text{ W/m}^2$ , alongside a mean flow velocity of  $0.61 \text{ m/s}$ , both of which likely contributed to substantial erosion and an overall net sediment loss of  $-14,772 \text{ m}^3$ . Sediment input from upstream was insufficient to compensate for this loss. In contrast, event B exhibited the lowest geomorphic activity, with a more balanced distribution of erosion and deposition across the river reach, resembling classical meander behaviour with distinct riffles and pools (Fig. 9B). Stream power during this event was considerably lower, predominantly below  $10 \text{ W/m}^2$ , with a mean flow velocity of  $0.36 \text{ m/s}$ . These conditions likely facilitated the deposition of eroded and transported sediment within the reach, resulting in a net sediment gain of  $5,482 \text{ m}^3$ .

Event C showed a relatively balanced response, with an even distribution of erosion and deposition, and the smallest net change, resulting in a sediment gain of  $1,132 \text{ m}^3$  (Fig. 9C). The upstream section experienced the greatest erosion, while sediment accumulation was most pronounced downstream. Only minor changes occurred in the middle reach based on the model. Stream power for event C was moderate, with values mostly below  $16 \text{ W/m}^2$  and only occasional exceedances above  $20 \text{ W/m}^2$ . Event D exhibited the most fragmented morphological response, with small, scattered areas of both erosion and deposition distributed throughout the reach (Fig. 9D). The stream power distribution for event D was more similar to that of event A, with values exceeding  $20 \text{ W/m}^2$  and a mean flow velocity of  $0.54 \text{ m/s}$ . Despite the relatively high energy, event D produced a more balanced sediment budget, though it still resulted in a net sediment loss of  $-6,267 \text{ m}^3$ . Geomorphic activity per unit area appeared highest for events A and D, both of which showed considerable sediment mobilisation but resulted in different morphological responses likely due to hydrograph shape. Events B and C exhibited lower geomorphic activity, with a tendency towards sediment deposition rather than erosion. The pattern of morphological change associated with the modelled flood events thus appeared to be linked to the peak shape, sequencing, and the resulting sediment transport hysteresis patterns, which collectively influenced the morphological response of bedforms.

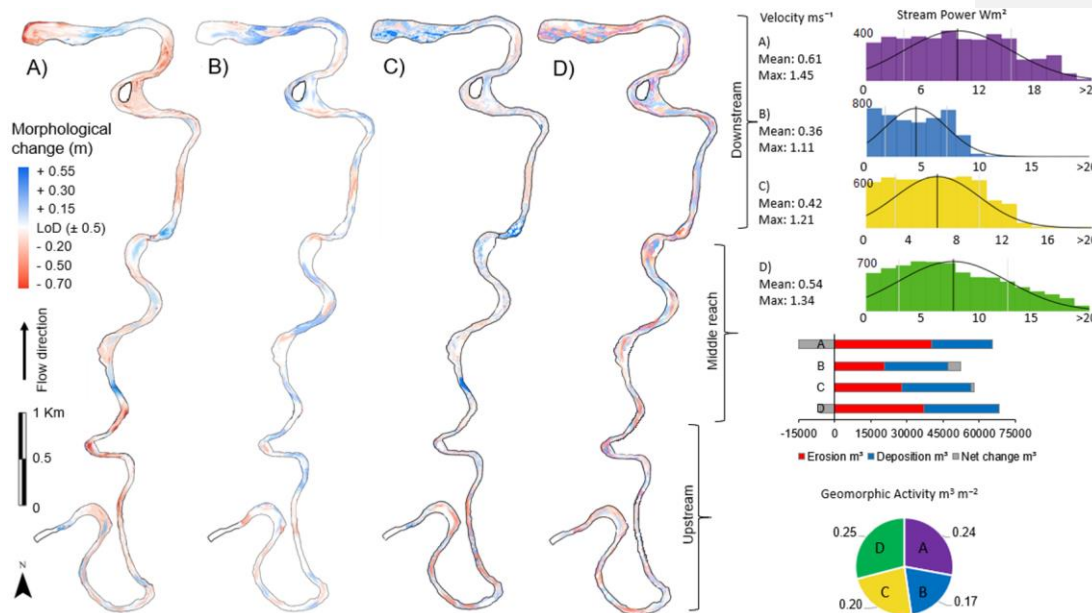


Figure 9. Morphological adjustment of each flood-event (A-D) in left panel: A) Distinct areas of heavy erosion and deposition. B) Desecrate morphological changes but distinct areas of erosion and deposition. C) More complex morphological changes patched around the river reach. D) Heavy erosion and deposition spread complexly inside the reach. Right panel: A-D events mean and max velocity, histograms of stream power (x) distribution within number of model cells (y), volume of erosion, deposition, and net change, and geomorphic activity.

## 5. Discussion

### 5.1. Flood-event types and hydroclimatic conditions

The results of variance analysis and trend test of climate variables and flood-event types aligned with well-documented responses to climate change in cold regions (Cockburn & Lamoureux, 2008; Vormoor et al., 2016; Matti et al., 2017; Arp et al., 2020). The significant increase in both mean and maximum spring temperatures matched global climate model predictions for continued warming at high-latitudes (Koenigk & Brodeau, 2017; Huo et al., 2022). The increased snow depth also aligned with Pulliainen et al. (2020), who reported rising snow accumulation and snow water equivalent (SWE) in the studied region. Despite this, no significant changes in flood volumes were observed, consistent with previous studies in Fennoscandia (Veijalainen et al., 2010; Korhonen & Kuusisto, 2010; Matti et al., 2017; Lintunen et al., 2024). This lack of change was attributed to milder winter conditions and longer snowmelt period resulting from warming temperatures, which lead to more stable runoff during spring (Fischer & Schumann, 2019; Zhang et al., 2023). Additionally, no significant trends were found in the timing, duration, or interval of flood-events, consistent

572 with earlier research in snowmelt-dominated regions (Veijalainen et al., 2010; Vormoor et  
573 al., 2016; Matti et al., 2017).

574

575 Despite the absence of significant trends, low-peak floods (B) increased in both volume and  
576 duration, while wavy floods (D) showed a reduction, respectively (Figure 7). Based on the  
577 results of ANOVA, both flood-events of this type were influenced by high annual temperature  
578 and high snow accumulation, but significantly different spring-time and May weather  
579 conditions. Events of type B experienced long and warm melt period during spring whereas  
580 events of type D were associated with late spring warmth with varying amounts of rainfall  
581 leading to non-uniform runoff. The climatic conditions associated with these event types are  
582 expected to intensify across the Northern Hemisphere (Callaghan et al., 2012; Kunkel et al.,  
583 2016; Conolly et al., 2019; Pulliainen et al., 2020; Hu et al., 2023), although climate change  
584 impact on snow accumulation is likely to vary spatially. These event types also exhibited an  
585 increase of re-occurrence-interval indicating that these flood-event types are likely to become  
586 more common in the future. High one-peak floods (A), however, were associated with cold,  
587 snow-rich years, where rapid warming in May leads to sharp and high flood hydrographs.  
588 This is consistent with findings that cold springs delay snowmelt and ground thaw, leading  
589 to high discharge peaks when the thaw eventually occurs (Labuhn et al., 2018). Unlike  
590 double-peaking floods, single-peak events involved lower temperatures and rainfall during  
591 spring, and therefore the rain-on-snow effect could be linked to the wetter conditions typical  
592 to events of type D. Even though events of type C are also double peaking, these  
593 hydrographs were linked to dry, mixed, or transitional climatic conditions, in which a  
594 particularly cold winter and spring lead to delayed snowmelt. Hydrographs of event type C  
595 had however, significant amount of rainfall in May which together with cold temperature  
596 conditions likely causes the two separate melt peaks typical to this event.

597 Climate change is expected to increase annual temperatures and to modify the precipitation  
598 patterns in high-latitude areas (Zhang et al., 2023; Blöschl et al., 2017). These changes will  
599 likely have an impact on the occurrence of certain flood-event types. Increased spring rainfall  
600 can increase rain-on-snow events significantly amplify runoff and flood peaks, particularly  
601 together with deep snow packs and accelerated snowmelt from warmer spring  
602 temperatures. Similar pattern have been recognized previously on high-latitudes by Fischer  
603 & Schumann (2019). The results observed in this study point to the direction of possible  
604 future hydroclimatic regime shift. These findings highlight the complex effects of climate  
605 change on flood-events and underscore the importance of considering flood-event  
606 sequencing in assessing the impacts of hydroclimatic shifts. Future research could explore  
607 climate teleconnections, such as the North Atlantic Oscillation (NAO) or Arctic Oscillation  
608 (AO), to better understand the conditions driving specific flood-events (Dahlke et al., 2012;  
609 Villarini et al., 2013; Irannezhad et al., 2022). In addition, it is worth of noting that while  
610 interpreting the results of this study, especially the results of ANOVA, the sample size has  
611 a critical impact on the reliability and validity of the results. Larger sample sizes increase the  
612 statistical power of the test, improving the ability to detect true differences between group  
613 means (Lakens, 2022). They also provide more precise estimates of means and variances,  
614 reduce the influence of outliers, and help satisfy the assumptions of normality and  
615 homogeneity of variances. In contrast, small samples can result in underpowered tests,

616 unstable F-statistics, and greater sensitivity to assumption violations, ultimately reducing the  
617 robustness of the findings

618

619

620

621

## 622 5.2. Flood-event types and morphological response

623 When interpreting the morphological results of the simulations in this study some limitations  
624 should be considered. As a depth-averaged model, it did not resolve vertical flow structures  
625 or secondary currents, which limit the capacity to fully represent sediment transport and bank  
626 erosion processes (Pinto et al., 2006; Nicholas et al., 2014; Williams et al., 2014). In addition,  
627 the model lacks the ability to simulate ice-covered flows and freeze–thaw effects, both of  
628 which significantly influence sediment dynamics and channel stability in cold-region rivers  
629 (Zhang et al., 2022). Model sensitivity to user-defined parameters, such as sediment  
630 fractions and roughness coefficients, further contributes to output uncertainty (Pinto et al.,  
631 2006). Moreover, the use of morphological acceleration factors and simplified boundary  
632 conditions may exaggerate or underrepresent morphological processes. Consequently,  
633 while the simulation runs presented in this study are effective in assessing relative  
634 differences between scenarios, caution is necessary when interpreting absolute sediment  
635 budgets and localised morphological changes due to simplifications, and the fact that it  
636 cannot simulate ice and freeze-thaw effect on sediment transport and bank erosion. In  
637 addition, only one hydrograph was modelled for each flood-event type, meaning that  
638 selecting a different hydrograph of the same type could have resulted in different volumetric  
639 changes and total amounts of transported sediment, as these depend on the flood’s volume  
640 and transport capacity. However, the findings of this study, together with previous laboratory  
641 (Mao, 2012; 2018) and modelling studies (Kasvi et al., 2015), support the view that the shape  
642 and sequence of the hydrograph play a crucial role in determining morphological outcomes.  
643 Therefore, it is likely that selecting different hydrographs for each flood-event type would  
644 have produced similar types of morphological patterns relative to the flood’s magnitude and  
645 transport capacity, even though the quantitative results may have differed.

646

647 Nevertheless, the model simulations showed that the channel bed’s morphological response  
648 was influenced by flood-event type and sequences, as well as sediment transport hysteresis  
649 pattern, rather than just flood magnitude. Similar finding have been made by Kasvi (2015)  
650 who found that the flood duration and flow characteristics have notable impact on channel  
651 morphology. All events exhibited dominant counterclockwise hysteresis, common in sand-  
652 bed rivers with upstream sediment supply and bedload-dominated transport (Tananev, 2015;  
653 Gunsolus & Binns, 2017). However, the riverbed’s morphological response varied depending  
654 on the modelled hydrograph shape. Single-peak events (A and B) produced distinct erosion  
655 and deposition patterns, while double-peaking events (C and D) led to fragmented, small-  
656 scale morphological features. Particularly, event B formed classic riffles and pools, typical to

meandering rivers (Hooke, 2003, Salmela et al., 2022), whereas the reduced sediment transport during second peaks in double-peaking events, also noted in previous flume experiments (Martin & Jerolmack, 2013; Mao, 2018), resulted in more complex, small-scale bedforms.

661

The reduction in sediment transport during the second flood peak has previously been linked to bed surface reorganisation, notably the exposure of coarser material (armouring) and infiltration of finer sediments (kinetic sieving), both of which stabilise the bed and increase the energy required for sediment remobilisation (Curran & Waters, 2014; Dudill et al., 2017; Ferdowsi et al., 2017; Mao, 2018). In contrast, event D displayed clockwise hysteresis during the second peak, suggesting that the bed did not fully stabilise between peaks, enabling more rapid sediment remobilisation and resulting in higher total transported sediment (TTS) compared to other flood events. This pattern may also indicate increased input of finer sediments from bank erosion, which tends to intensify during the falling limb of the hydrograph as water levels decline (Lotsari et al., 2014; Lotsari et al., 2024; Yang et al., 2024). Bank erosion dynamics are further influenced by freeze-thaw processes and the presence of seasonally frozen ground, which the current model does not represent. The thermal condition of banks and bars during different flood stages strongly affects erosion rates, with thawed banks being considerably more erodible than frozen ones (Lotsari et al., 2024; van Rooijen & Lotsari, 2024; Yang et al., 2024). Moreover, both soil moisture and the number of freeze-thaw cycles reduce bank stability (Li et al., 2022; Lotsari et al., 2024). As climate change is expected to prolong freeze-thaw periods (Blåfield et al., 2024a; Sha et al., 2025), future bank erosion rates and sediment fluxes are likely to increase. Additionally, enhanced cold-season discharge and earlier freshet onset under warmer conditions will further promote riverbank erosion in many regions (Brown et al., 2020).

~~The reduction in sediment transport during the second flood peak has been previously attributed to bed surface reorganization, including coarser sediment exposure (armouring) and infiltration of finer sediments (kinetic sieving), which stabilises the bed, requiring more energy for remobilisation (Curran & Waters, 2014; Dudill et al., 2017; Ferdowsi et al., 2017; Mao, 2018). However, event D displayed clockwise hysteresis during the second peak, suggesting that the riverbed was not able to stabilise between the peaks, enabling faster remobilization of sediments during the second peak and therefore higher TTS compared to other flood events. This can also be a sign of finer sediment contribution due to bank erosion as bank erosion and slumping/mass failures increase as the water level decreases (Lotsari et al., 2014; Lotsari et al., 2024; Yang et al., 2024). This is further impacted by freeze-thaw cycles and seasonally frozen ground, which the model used in this study however, cannot replicate. Whether the bank or bars are frozen during the rising, peaking and falling limb of the flood has significant impact on the amount of erosion (Lotsari et al., 2024; van Rooijen & Lotsari, 2024; Yang et al., 2024) as thawing banks have higher erosion magnitude compared to frozen banks. In addition, the moisture content and amount of freeze-thaw cycles affects the erodibility of the soil by reducing bank stability (Li et al., 2022; Lotsari et al., 2024). This is a factor which likely has significant impact on bank erosion rates and sediment flux volumes in the future as previous studies have noted that the freeze-thaw cycles are prolonged due to climate change (Blåfield et al., 2024a; Sha et al., 2025). In addition to~~

Formatted: English (United Kingdom)



701 prolonged freeze-thaw cycle, increased cold season discharge and earlier freshet occurring  
702 under warmer conditions enhance riverbank erosion in most areas (Brown et al., 2020).

703

704 The fragmented bedforms from double-peaking floods were likely caused by secondary  
705 bedforms cannibalizing the larger topography from the first peak, a phenomenon observed  
706 in flume studies (Wilbers & Brinke, 2003; Martin et al., 2013). In addition to flood hydrograph  
707 shape and hysteresis pattern, sediment particle size played a key role in morphological  
708 adjustment. The middle reach with the largest particles (Fig. 5) was eroded mainly during  
709 events A and D, while events B and C caused minimal change in this section of the river.  
710 This finding was consistent with earlier research on particle size impact on sediment  
711 transport hysteresis and remobilisation of the sediment particles (Mao, 2012; Malutta et al.,  
712 2020). Despite variations in the modelled runoff volumes, the study identified distinct  
713 morphological response patterns for each flood-event type. These patterns, shaped by  
714 sediment transport hysteresis, distribution of sediment particle size and flood-event  
715 sequences, align with findings from previous studies (Martin & Jerolmack, 2013; Gunsolus  
716 & Binns, 2017; Mao, 2018). The results highlighted the crucial role of different flood-event  
717 types in shaping river morphology, revealing that, while event variation likely helps maintain  
718 channel equilibrium in long-term, prolonged exposure to certain events—such as high-  
719 energy or multi-peaking floods—could disrupt this balance. Such evolution have the potential  
720 to destabilise the channel, by altering sediment connectivity, transport processes, and  
721 ultimately the morphological structure of the river systems (Bracken et al., 2015; Zhang et  
722 al., 2023). Understanding these responses is essential for predicting future river behaviour  
723 and managing morphological stability.

724

### 725 5.3. Forecasted hydroclimatic shift and long-term morphological adjustment

726 This study highlighted the importance of understanding how fluvial sand and gravel-bed  
727 systems respond to climatic conditions, particularly by examining the sequences of flood  
728 hydrographs, which are often overlooked, and more focus is paid on factors like flood  
729 volume, timing, or frequency. The results revealed that flood-event type and peak  
730 sequencing had significant impact on the morphological response of the channel. This  
731 together with the observed trends, suggested that even in regions, like the one studied,  
732 where hydroclimatic changes are not yet fully visible (Veijalainen et al., 2010; Lintunen et al.,  
733 2024), flood-event characteristics are evolving with consequences to the river morphology.  
734 This and the overserved trends in the hydroclimatic variables underscores that hydroclimatic  
735 change is not uniform in space and time across cold regions and rivers should be assessed  
736 at the catchment scale to predict future morphological adjustment accurately.

737

738 The increase (decrease) of double (single) peaking floods could lead to changes in river  
739 system stability, sediment loads, and in the spatial distribution of long-term morphological  
740 adjustment if certain type of morphological response begin to accumulate (Bracken et al.,  
741 2015; Zhang et al., 2023; Blåfield et al., 2024a). Furthermore, previous research findings  
742 suggesting that sediment loads in cold regions could rise by 20-30 % for every 1-2 °C  
743 increase in temperature (Syvitski et al., 2002; Li et al., 2021) was supported by this study,

as the double-peaking floods related to warmer annual temperatures, showed higher geomorphic activity and sediment loads compared to single peaking events of similar volume. The temperature increase together with altered morphological response pattern could eventually lead to sediment transport regime shift. However, the anticipated shift is likely to be a gradual process (Zhang et al., 2023), and the river system may eventually stabilise again. Yet, before stabilizing the shift is likely to challenge the river channel stability, making the long-term morphological adjustment, like meander migration, less predictable (Wohl et al., 2017; Hopwood et al., 2021).

752

Shifts in the sediment transport regime, along with changes in morphological response and long-term adjustment to evolving flood patterns, are likely to influence the morphological response to summer and autumn precipitation by altering sediment availability and bed form composition. Although these precipitation peaks were not the focus of this study, these seasonal peaks should be considered when predicting and evaluating long-term morphological adjustment of river channels as the distribution of seasonal sediment load is likely shifting towards summer and autumn peaks (Li et al., 2021; Zhang et al., 2023; Blåfield et al., 2024a). This could have significant implications for river ecosystems, flood risk management, and infrastructure planning (Beel., et al., 2021; Gupta et al., 2021; Najafi et al., 2021). As discharge regimes become increasingly event-driven rather than seasonally predictable, traditional models of sediment flux that assume clear seasonal patterns may no longer be applicable. Hysteresis patterns, where sediment concentration and water discharge are no longer linearly related, can reveal critical thresholds, sediment sources, and system memory that are key to predicting future river behaviour. Therefore, future research should focus on understanding the combined effects of flood-event sequencing, changing precipitation patterns, and sediment transport dynamics under evolving climatic conditions. Long-term monitoring and advanced modelling efforts will be essential to predict the future morphological adjustments of rivers and develop strategies for mitigating these changes' impacts on ecological systems.

772

## 773 6. Conclusions

774

The findings of this study emphasise the critical role that flood-event variability and sequencing play in shaping the morphological response of fluvial sand and gravel-bed systems in cold regions. The results demonstrated that even in areas where hydroclimatic changes are not yet fully visible, flood-event characteristics are evolving and remain closely linked to specific climatic conditions. Each flood-event type produced distinct morphological responses, such as the formation of riffles and pools during single-peaking floods, and more fragmented and irregular bed forms in double-peaking floods. Additionally, sediment grain size significantly influenced the spatial distribution of erosion and deposition. The increase of double-peaking flood-events, coupled with rising temperatures, could lead to a shift in sediment transport regimes, resulting in heightened geomorphic activity and altered sediment loads. The results underscore the importance of assessing hydroclimatic conditions and flood hydrograph sequences at the catchment scale to accurately predict future morphological adjustment as the impacts of hydroclimatic shift are not uniform across

788 the arctic. Future research should focus on the combined impacts of flood sequences,  
789 precipitation patterns, and sediment transport dynamics to develop effective strategies for  
790 managing the evolving river systems under climate change. These changes are expected  
791 to affect long-term river stability, with significant implications for river ecosystems and flood  
792 risk management.

793

794 **Data availability**

795 The climate data is openly available on Finnish Meteorological Institutes (FMI) data service.  
796 The Polmak discharge station data is openly available on Norwegian Water Resources and  
797 Energy Directorate (NVE) data service. All the other data is available on request.

798

799 **Author contribution**

800 Linnea Blåfield – Writing the manuscript, Field work, Methodology, Formal analysis,  
801 Visualisation, Funding.

802 Carlos Gonzales-Inca – Formal analysis, Editing the manuscript

803 Petteri Alho – Field work, Data curation, Resources, Reviewing the manuscript, Funding,  
804 Supervision

805 Elina Kasvi – Field work, Reviewing the manuscript, Funding, Supervision

806

807 **Declaration of competing interest**

808 The authors declare that they have no conflict of interest.

809

810 **Funding**

811 This study was funded by the Kone Foundation (202104246), AnthroCliMocs (355018), and  
812 by the European Union's Next Generation EU recovery instrument (RRF) through the  
813 Research Council of Finland projects: HYDRO-RDI-Network (337279), Green-Digi-Basin  
814 (347701), and HYDRO-RI-platform (346161). The study received support also from the  
815 Flagship Programme funding granted by the Research Council of Finland for Digital Waters  
816 – DIWA Flagship (359247).

817

818

819

820 **Acknowledgements**

821 The authors would like to thank research assistant Oona Oksanen from the Fluvial and  
822 Coastal Research Group (University of Turku) for helping with the data processing, and  
823 other group members who have participated in the field work.  
824

825  
826 **References**

827 Arp, C. D., Whitman, M. S., Kemnitz, R., & Stuefer, S. L.:Evidence of hydrological  
828 intensification and regime change from northern Alaskan watershed runoff.  
829 Geophysical Research Letters, 47(17), e2020GL089186.  
830 <https://doi.org/10.1029/2020GL089186>, 2020.  
831 Beel, C. R, et al.: Emerging dominance of summer rainfall driving High Arctic terrestrial-  
832 aquatic connectivity. Nat. Commun. 12, 1448 [https://doi.org/10.1038/s41467-021-](https://doi.org/10.1038/s41467-021-21759-3)  
833 [21759-3](https://doi.org/10.1038/s41467-021-21759-3), 2021.  
834 Blåfield, L., Marttila, H., Kasvi, E., & Alho, P.: Temporal shift of hydroclimatic regime and its  
835 influence on migration of a high latitude meandering river. Journal of Hydrology, 633,  
836 130935. <https://doi.org/10.1016/j.jhydrol.2024.130935>, 2024a.  
837 Blåfield, L., Calle, M., Kasvi, E., & Alho, P.: Modelling seasonal variation of sediment  
838 connectivity and its interplay with river forms. Geomorphology, 463, 109346.  
839 <https://doi.org/10.1016/j.geomorph.2024.109346>, 2024b.  
840 Blöschl, G et al.: Changing climate shifts timing of European floods.Science357,588-  
841 590(2017). DOI:10.1126/science.aan2506, 2017.  
842 Bracken, L. J., Turnbull, L., Wainwright, J., & Bogaart, P.: Sediment connectivity: a  
843 framework for understanding sediment transfer at multiple scales. Earth surface  
844 processes and landforms, 40(2), 177-188. <https://doi.org/10.1002/esp.3635>, 2015.  
845 Brown, D.R.N., Brinkman, T.J., Bolton, W.R. et al., Implications of climate variability and  
846 changing seasonal hydrology for subarctic riverbank erosion. Climatic Change,162,  
847 1–20, <https://doi.org/10.1007/s10584-020-02748-9>, 2020.  
848 Callaghan, T.V., Johansson, M., Brown, R.D. et al.: The Changing Face of Arctic Snow  
849 Cover: A Synthesis of Observed and Projected Changes. AMBIO 40 (Suppl 1), 17–  
850 31. <https://doi.org/10.1007/s13280-011-0212-y>, 2011.  
851 Cockburn, J. M., & Lamoureux, S. F.: Hydroclimate controls over seasonal sediment yield  
852 in two adjacent High Arctic watersheds. Hydrological Processes: An International  
853 Journal, 22(12), 2013-2027. <https://doi.org/10.1002/hyp.6798>, 2008.  
854 Connolly R 1, Connolly M, Soon W, Legates DR, Cionco RG, Velasco Herrera VM. Northern  
855 Hemisphere Snow-Cover Trends (1967–2018): A Comparison between Climate  
856 Models and Observations. Geosciences. 9(3):135.  
857 <https://doi.org/10.3390/geosciences90301>, 2019.  
858 Curran, J. C., Waters, K. A., & Cannatelli, K. M.: Real time measurements of sediment  
859 transport and bed morphology during channel altering flow and sediment transport  
860 events. Geomorphology, 244, 169-179.,  
861 <https://doi.org/10.1016/j.geomorph.2015.03.009>, 2015.  
862 Daneshvar Vousoughi, F., Dinpashoh, Y., Aalami, M.T., Jhajaharia ,D.: Trend analysis of  
863 groundwater using non-parametric methods (case study: Ardabil plain) Stochastic  
864 Environ. Res. Rsk Assessm., 27 (2013), pp. 547-559, DOI: 10.1007/s00477-012-  
865 0599-4, 2013.

Formatted: Font color: Text 1

Formatted: Font: (Default) Arial, 12 pt, Font color: Text 1

Formatted: Font: (Default) Arial, Font color: Text 1

Formatted: Font color: Text 1

Formatted: Font: (Default) Arial, 12 pt, Font color: Text 1

Formatted: Font: (Default) Arial, Font color: Text 1

Formatted: Font color: Text 1

Formatted: Font color: Text 1

Formatted: Font color: Text 1

Formatted: Font color: Text 1

Formatted: Font color: Text 1

Formatted: Font: (Default) Arial, 12 pt, Font color: Text 1

Formatted: Font color: Text 1

Formatted: Font color: Text 1

Formatted: Font color: Text 1

Formatted: Font: Not Italic, Font color: Text 1

Formatted: Font color: Text 1

Formatted: Font: Not Italic, Font color: Text 1

Formatted: Font color: Text 1

Formatted: Font: Not Bold, Font color: Text 1

Formatted: Font color: Text 1

Formatted: Font color: Text 1

Formatted: Font color: Text 1

Formatted: Font color: Text 1

Formatted: Font color: Text 1

Formatted: Font color: Text 1

Formatted: Font color: Text 1

Formatted: Font color: Text 1

Formatted: Font color: Text 1

Formatted: Font: (Default) Arial, 12 pt, Font color: Text 1

Formatted: Font: (Default) Arial, 12 pt, Font color: Text 1

Formatted: Font: (Default) Arial, Font color: Text 1

Formatted: Font color: Text 1



912 [Jhajharia, D., Dinpashoh, Y., Kahya, E., Choudhary, R. R., & Singh, V. P. \(2014\). Trends in](#)  
913 [temperature over Godavari River basin in Southern Peninsular India. International](#)  
914 [Journal of Climatology, 34\(5\). DOI: 10.1002/joc.3761, 2014.](#)

915 [Johansson, P.: Late Weichselian deglaciation in Finnish Lapland. Applied Quaternary](#)  
916 [research in the central part of glaciated terrain, 47, 2007.](#)

917 [Kasvi, E., Alho, P., Lotsari, E., Wang, Y., Kukko, A., Hyypä, H., & Hyypä, J.: Two-](#)  
918 [dimensional and three-dimensional computational models in hydrodynamic and](#)  
919 [morphodynamic reconstructions of a river bend: sensitivity and functionality.](#)  
920 [Hydrological processes, 29\(6\), 1604-1629. https://doi.org/10.1002/hyp.10277, 2015.](#)

921 [Karimae Tabarestani, M., Zarrati, A.R.: Sediment transport during flood-event: a review.](#)  
922 [Int. J. Environ. Sci. Technol. 12, 775–788, https://doi.org/10.1007/s13762-014-0689-](#)  
923 [6, 2015.](#)

924 [Kociuba, W.: The Role of Bedload Transport in the Development of a Proglacial River](#)  
925 [Alluvial Fan \(Case Study: Scott River, Southwest Svalbard\). Hydrology, 8\(4\), 173.](#)  
926 [https://doi.org/10.3390/hydrology8040173, 2021.](#)

927 [Korhonen, J., & Kuusisto, E.: Long-term changes in the discharge regime in Finland.](#)  
928 [Hydrology Research, 41\(3-4\), 253-268. https://doi.org/10.2166/nh.2010.112, 2010.](#)

929 [Kunkel, K.E., Robinson, D.A., Champion, S. et al. Trends and Extremes in Northern](#)  
930 [Hemisphere Snow Characteristics. Curr Clim Change Rep 2, 65–73,](#)  
931 [https://doi.org/10.1007/s40641-016-0036-8, 2016.](#)

932 [Labuhn, I., Hammarlund, D., Chapron, E., Czymzik, M., Dumoulin, J. P., Nilsson, A., ... &](#)  
933 [Von Grafenstein, U.: Holocene hydroclimate variability in central Scandinavia inferred](#)  
934 [from flood layers in contourite drift deposits in Lake Storsjön. Quaternary, 1\(1\), 2.](#)  
935 [2018.](#)

936 [Lakens, D.: Sample size justification. Collabra: Psychology, 8\(1\), 33267.](#)  
937 [https://doi.org/10.1525/collabra.33267, 2022.](#)

938 [Li, C., Yang, Z., Shen, H. T., & Mou, X.: Freeze-Thaw Effect on Riverbank Stability. Water,](#)  
939 [14\(16\), 2479. https://doi.org/10.3390/w14162479, 2022.](#)

940 [Li, D., Overeem, I., Kettner, A. J., Zhou, Y., & Lu, X.: Air temperature regulates erodible](#)  
941 [landscape, water, and sediment fluxes in the permafrost-dominated catchment on the](#)  
942 [Tibetan Plateau. Water Resources Research, 57\(2\),](#)  
943 [https://doi.org/10.1029/2020WR028193, 2021.](#)

944 [Liébault, F., Laronne, J. B., Klotz, S., & Bel, C.: Seasonal bedload pulses in a small alpine](#)  
945 [catchment. Geomorphology, 398, 108055.](#)  
946 [https://doi.org/10.1016/j.geomorph.2021.108055, 2022.](#)

947 [Lintunen, K., Kasvi, E., Uvo, C. B., & Alho, P.: Changes in the discharge regime of Finnish](#)  
948 [rivers. Journal of Hydrology: Regional Studies, 53, 101749,](#)  
949 [https://doi.org/10.1016/j.ejrh.2024.101749, 2024.](#)

950 [Lotsari, E., Hackney, C., Salmela, J., Kasvi, E., Kemp, J., Alho, P., and Darby, S. E.: Subarctic river bank dynamics and driving processes during the open-channel flow](#)  
951 [period. Earth Surf. Process. Landforms, 45: 1198–1216.](#)  
952 [https://doi.org/10.1002/esp.4796, 2020.](#)

953 [Lotsari, E., Dietze, M., Kämäri, M., Alho, P., & Kasvi, E.: Macro-Turbulent flow and its](#)  
954 [impacts on sediment transport potential of a subarctic river during ice-covered and](#)  
955 [open-channel conditions. Water, 12\(7\), 1874. https://doi.org/10.3390/w12071874,](#)  
956 [2020.](#)

957

Formatted

Formatted: Font: (Default) Arial, 12 pt, Font color: Text

Formatted

Formatted

Formatted

Formatted: Font: (Default) Arial, 12 pt, Font color: Text

Formatted

Formatted: Font: (Default) Arial, 12 pt, Font color: Text

Formatted

Formatted: Font color: Text 1

Formatted: Font color: Text 1

Formatted

Formatted

Formatted

Formatted

Formatted: Font color: Text 1

Formatted: Font: (Default) Arial, 12 pt, Font color: Text

Formatted

Formatted: Font: (Default) Arial, 12 pt, Font color: Text

Formatted

Formatted

Formatted

Formatted

Formatted: Font color: Text 1

Formatted

Formatted: Font color: Text 1, Finnish



958 Lotsari, E., Vaaja, M., Flener, C., Kaartinen, H., Kukko, A., Kasvi, E., ... & Alho, P.: Annual  
959 bank and point bar morphodynamics of a meandering river determined by high-  
960 accuracy multitemporal laser scanning and flow data. Water Resources Research,  
961 50(7), 5532-5559. <https://doi.org/10.1002/2013WR014106>, 2014,  
962 Lotsari, E., de Vet, M., Murphy, B., McLelland, S., and Parsons, D.: Defrosting river banks:  
963 morphodynamics and sediment flux, EGU General Assembly 2024, Vienna, Austria,  
964 14–19 Apr 2024, EGU24-10175, <https://doi.org/10.5194/egusphere-equ24-10175>,  
965 2024.  
966 Luoto, M., Heikkinen, R.K. and Carter, T.R.: Loss of palsa mires in europe and biological  
967 consequences. Environmental conservation, 31(1), pp. 30–37.  
968 Doi:10.1017/s0376892904001018, 2004.  
969 Malutta, S. Kobiyama, M. Borges Chaffe, P-L. Bernardi Bonumá, N; Hysteresis analysis to  
970 quantify and qualify the sediment dynamics: state of the art. Water Science  
971 Technology; 81 (12): 2471–2487, <https://doi.org/10.2166/wst.2020.279>, 2020,  
972 Mao, L.: The effect of hydrographs on bed load transport and bed sediment spatial  
973 arrangement, J. Geophys. Res. 117, F03024,. doi:10.1029/2012JF002428, 2012.  
974 Mao, L.: The effects of flood history on sediment transport in gravel-bed rivers.  
975 Geomorphology, 322, 196-205. <https://doi.org/10.1016/j.geomorph.2018.08.046>,  
976 2018.  
977 Matti, B., Dahlke, H., Dieppois, B., Lawler, D., & Lyon, S.: Flood seasonality across  
978 Scandinavia—Evidence of a shifting hydrograph? Hydrological Processes, 31(24),  
979 4354-4370. <http://dx.doi.org/10.1002/hyp.11365>, 2017.  
980 Martin, R. L. and D. J. Jerolmack: Origin of hysteresis in bed form response to unsteady  
981 flows, Water Resour. Res. 49, 1314–1333,. doi:10.1002/wrcr.20093, 2013.  
982 Meriö, L. J., Ala-aho, P., Linjama, J., Hjort, J., Kløve, B., & Marttila, H. (2019). Snow to  
983 precipitation ratio controls catchment storage and summer flows in boreal headwater  
984 catchments. Water Resources Research, 55(5), 4096-4109.  
985 Micheletti, N., Chandler, J., & Lane, S.: Near instantaneous production of digital terrain  
986 models in the field using smartphone and Structure-from-Motion photogrammetry. In  
987 EGU General Assembly Conference Abstracts (pp. EGU2013-10501), 2013.  
988 Mohammadzadeh Khani H, Kinnard C, Lévesque E.: Historical Trends and Projections of  
989 Snow Cover over the High Arctic: A Review. Water. 14(4):587.  
990 <https://doi.org/10.3390/w14040587>, 2022,  
991 Najafi, S., Dragovich, D., Heckmann, T., & Sadeghi, S. H.: Sediment connectivity concepts  
992 and approaches. Catena, 196, 104880.  
993 <https://doi.org/10.1016/j.catena.2020.104880>, 2021,  
994 Tananaev, N. I: Hysteresis effects of suspended sediment transport in relation to  
995 geomorphic conditions and dominant sediment sources in medium and large rivers  
996 of the Russian Arctic. Hydrology Research 1 April 2015; 46 (2): 232–243,  
997 <https://doi.org/10.2166/nh.2013.199>, 2015,  
998 Phillips, C. B., Hill, K. M., Paola, C., Singer, M. B., & Jerolmack, D. J.: Effect of flood  
999 hydrograph duration, magnitude, and shape on bed load transport dynamics.  
1000 Geophysical Research Letters, 45, 8264–8271.  
1001 <https://doi.org/10.1029/2018GL078976>, 2018,  
1002 Pulliainen, J., Luojus, K., Derksen, C. et al.: Patterns and trends of Northern Hemisphere  
1003 snow mass from 1980 to 2018. Nature 581, 294–298, [https://doi.org/10.1038/s41586-](https://doi.org/10.1038/s41586-020-2258-0)  
1004 020-2258-0, 2020,

Formatted: Font color: Text 1

Formatted: Font: (Default) Arial, 12 pt, Font color: Text

Formatted: Font: (Default) Arial, Font color: Text 1

Formatted: Font color: Text 1

Formatted: Font: (Default) Arial, 12 pt, Font color: Text

Formatted: Font: (Default) Arial, 12 pt, Font color: Text

Formatted: Font: (Default) Arial, Font color: Text 1

Formatted: Font color: Text 1

Formatted: Font: (Default) Arial, 12 pt, Font color: Text

Formatted: Font: (Default) Arial, 12 pt, Font color: Text

Formatted: Font color: Text 1

Formatted: Font color: Text 1

Formatted: Font color: Text 1

Formatted: Font color: Text 1, Swedish (Sweden)

Formatted: Font color: Text 1

Formatted: Font color: Text 1, Swedish (Sweden)

Formatted: Font color: Text 1

Formatted: Font: (Default) Arial, 12 pt, Font color: Text

Formatted: Font: (Default) Arial, Font color: Text 1

Formatted: Font color: Text 1

Formatted: Font: (Default) Arial, 12 pt, Font color: Text

Formatted: Font: (Default) Arial, Font color: Text 1

Formatted: Font color: Text 1

Formatted: Font: (Default) Arial, 12 pt, Font color: Text

Formatted: Font: (Default) Arial, 12 pt, Font color: Text

Formatted: Font: (Default) Arial, Font color: Text 1

Formatted: Font color: Text 1

Formatted: Font: (Default) Arial, 12 pt, Font color: Text

Formatted: Font: (Default) Arial, Font color: Text 1

Formatted: Font color: Text 1

Formatted: Font: (Default) Arial, 12 pt, Font color: Text

Formatted: Font: (Default) Arial, 12 pt, Font color: Text

Formatted: Font color: Text 1



1005 Reesink, A. J., & Bridge, J. S.: Evidence of bedform superimposition and flow unsteadiness  
1006 in unit-bar deposits, South Saskatchewan River, Canada. Journal of Sedimentary  
1007 Research, 81(11), 814-840, <https://doi.org/10.2110/jsr.2011.69>, 2011.

1008 Salmela, J., Kasvi, E., Vaaja, M. T., Kaartinen, H., Kukko, A., Jaakkola, A., & Alho, P.:  
1009 Morphological changes and riffle-pool dynamics related to flow in a meandering river  
1010 channel based on a 5-year monitoring period using close-range remote sensing.  
1011 Geomorphology, 352, 106982. <https://doi.org/10.1016/j.geomorph.2019.106982>,  
1012 2020.

1013 Sen, P. K.: Estimates of the regression coefficient based on Kendall's tau. Journal of the  
1014 American statistical association, 63(324), 1379-1389.  
1015 <https://doi.org/10.1080/01621459.1968.10480934>, 1968.

1016 Syvitski, J. P.: Sediment discharge variability in Arctic rivers: implications for a warmer  
1017 future. Polar Research, 21(2), 323-330. <https://doi.org/10.3402/polar.v21i2.6494>,  
1018 2020.

1019 Shrestha, R.R., Bennett, K.E., Peters, D.L., Yang, D.: Hydrologic Extremes in Arctic Rivers  
1020 and Regions: Historical Variability and Future Perspectives. In: Yang, D., Kane, D.L.  
1021 (eds) Arctic Hydrology, Permafrost and Ecosystems. Springer, Cham. 2021.

1022 van Rooijen, E., & Lotsari, E., 2024 The spatiotemporal distribution of river bank erosion  
1023 events and their drivers in seasonally frozen regions, Geomorphology, Volume 454.  
1024 <https://doi.org/10.1016/j.geomorph.2024.109140>, 2024.

1025 Vatne, G., Takøy Naas, Ø., Skårholen, T., Beylich, A. A., & Berthling, I.: Bed load transport  
1026 in a steep snowmelt-dominated mountain stream as inferred from impact sensors.  
1027 Norsk Geografisk Tidsskrift-Norwegian Journal of Geography, 62(2), 66-74.  
1028 <https://doi.org/10.1080/00291950802094817>, 2008.

1029 Veijalainen, N., Lotsari, E., Alho, P., Vehviläinen, B., & Käyhkö, J.: National scale  
1030 assessment of climate change impacts on flooding in Finland. Journal of hydrology,  
1031 391(3-4), 333-350, <https://doi.org/10.1016/j.jhydrol.2010.07.035>, 2010.

1032 Viglione, A., Chirico, G. B., Komma, J., Woods, R., Borga, M., & Blöschl, G.: Quantifying  
1033 space-time dynamics of flood-event types. Journal of Hydrology, 394(1-2), 213-229.  
1034 <https://doi.org/10.1016/j.jhydrol.2010.05.041>, 2010.

1035 Vormoor, K., Lawrence, D., Schlichting, L., Wilson, D., & Wong, W. K.: Evidence for changes  
1036 in the magnitude and frequency of observed rainfall vs. snowmelt driven floods in  
1037 Norway. Journal of Hydrology, 538, 33-48.  
1038 <https://doi.org/10.1016/j.jhydrol.2016.03.066>, 2016.

1039 Wenng, H., Barneveld, R., Bechmann, M., Marttila, H., Krogstad, T., & Skarbøvik, E.:  
1040 Sediment transport dynamics in small agricultural catchments in a cold climate: a  
1041 case study from Norway. Agriculture, Ecosystems & Environment, 317, 107484.  
1042 <https://doi.org/10.1016/j.agee.2021.107484>, 2021.

1043 Williams, G. P.: Sediment concentration versus water discharge during single hydrologic  
1044 events in rivers. Journal of Hydrology, 111(1-4), 89-106.  
1045 [https://doi.org/10.1016/0022-1694\(89\)90254-0](https://doi.org/10.1016/0022-1694(89)90254-0), 1989.

1046 Wohl, E.: Connectivity in rivers. Progress in Physical Geography, 41(3), 345-362.  
1047 <https://doi.org/10.1177/030913317714972>, 2017.

1048 Zhang, T., Li, D., Kettner, A. J., Zhou, Y., & Lu, X.: Constraining dynamic sediment-discharge  
1049 relationships in cold environments: The sediment-availability-transport (SAT) model.  
1050 Water Resources Research, 57(10), <https://doi.org/10.1029/2021WR030690>, 2021.

Formatted

Formatted

Formatted

Formatted

Formatted: Font: (Default) Arial, 12 pt, Font color: Text

Formatted

Formatted: Font: (Default) Arial, 12 pt, Font color: Text

Formatted

Formatted

Formatted: Font: (Default) Arial, Font color: Text 1

Formatted: Font color: Text 1

Formatted

Formatted: Font color: Text 1

Formatted

Formatted

Formatted: Font: (Default) Arial, 12 pt, Font color: Text

Formatted

Formatted: Font: (Default) Arial, 12 pt, Font color: Text

Formatted

Formatted: Font: (Default) Arial, 12 pt, Font color: Text

Formatted

Formatted: Font: (Default) Arial, 12 pt, Font color: Text

Formatted

Formatted: Font: (Default) Arial, 12 pt, Font color: Text

Formatted

Formatted

Formatted

1052 Zhang, T., Li, D., East, A.E. et al. Warming-driven erosion and sediment transport in cold  
1053 regions. *Nat Rev Earth Environ* 3, 832–851, [https://doi.org/10.1038/s43017-022-](https://doi.org/10.1038/s43017-022-00362-0)  
1054 [00362-0](https://doi.org/10.1038/s43017-022-00362-0), 2022.

1055 Zhang, T., Li, D., East, A. E., Kettner, A. J., Best, J., Ni, J., & Lu, X.: Shifted sediment-  
1056 transport regimes by climate change and amplified hydrological variability in  
1057 cryosphere-fed rivers. *Science Advances*, 9(45). DOI: 10.1126/sciadv.adi5019, 2023.

1058

1059 **References**

1060 Arp, C. D., Whitman, M. S., Komnitz, R., & Stuefer, S. L. (2020). Evidence of hydrological  
1061 intensification and regime change from northern Alaskan watershed runoff. *Geophysical*  
1062 *Research Letters*, 47(17), e2020GL089186.

1063 Beel, C. R., et al., (2012) Emerging dominance of summer rainfall driving High Arctic  
1064 terrestrial–aquatic connectivity. *Nat. Commun.* 12, 1448 (2021).

1065 Blåfield, L., Marttila, H., Kasvi, E., & Alho, P. (2024a). Temporal shift of hydroclimatic  
1066 regime and its influence on migration of a high latitude meandering river. *Journal of*  
1067 *Hydrology*, 633, 130935. <https://doi.org/10.1016/j.jhydrol.2024.130935>

1068 Blåfield, L., Calo, M., Kasvi, E., & Alho, P. (2024b). Modelling seasonal variation of  
1069 sediment connectivity and its interplay with river forms. *Geomorphology*, 463, 109346.  
1070 <https://doi.org/10.1016/j.geomorph.2024.109346>

1071 Blöschl, G. et al., Changing climate shifts timing of European floods. *Science* 357, 588–  
1072 590 (2017). DOI:10.1126/science.aan2506

1073 Bracken, L. J., Turnbull, L., Wainwright, J., & Bogaart, P. (2015). Sediment connectivity: a  
1074 framework for understanding sediment transfer at multiple scales. *Earth surface processes*  
1075 *and landforms*, 40(2), 177–188. <https://doi.org/10.1002/esp.3635>

1076 Brown, D.R.N., Brinkman, T.J., Bolton, W.R. et al. Implications of climate variability and  
1077 changing seasonal hydrology for subarctic riverbank erosion. *Climatic Change* **162**, 1–20  
1078 (2020). <https://doi.org/10.1007/s10584-020-02748-9>

1079 Callaghan, T.V., Johansson, M., Brown, R.D. et al. The Changing Face of Arctic Snow  
1080 Cover: A Synthesis of Observed and Projected Changes. *AMBIO* 40 (Suppl 1), 17–31  
1081 (2011). <https://doi.org/10.1007/s13280-011-0212-y>

1082 Cockburn, J. M., & Lamoureux, S. F. (2008). Hydroclimate controls over seasonal  
1083 sediment yield in two adjacent High Arctic watersheds. *Hydrological Processes: An*  
1084 *International Journal*, 22(12), 2013–2027. <https://doi.org/10.1002/hyp.6798>

1085 Connolly R 1, Connolly M, Soon W, Legates DR, Cionco RG, Velasco Herrera VM.  
1086 Northern Hemisphere Snow Cover Trends (1967–2018): A Comparison between Climate  
1087 Models and Observations. *Geosciences*. 2019; 9(3):135.  
1088 <https://doi.org/10.3390/geosciences90301>

1089 Curran, J. C., Waters, K. A., & Cannatelli, K. M. (2015). Real time measurements of  
1090 sediment transport and bed morphology during channel altering flow and sediment  
1091 transport events. *Geomorphology*, 244, 169–179.

1092 Daneshvar Vouseoughi, F., Dinpashoh, Y., Aalami, M.T., Jhajharia, D. (2013). Trend  
1093 analysis of groundwater using non-parametric methods (case study: Ardabil plain)  
1094 *Stochastic Environ. Res. Rsk Assessm.*, 27 (2013), pp. 547–559, DOI: 10.1007/s00477-  
1095 012-0599-4

1096 Fischer, S., Schumann, A. Spatio-temporal consideration of the impact of flood event  
1097 types on flood statistic. *Stoch Environ Res Risk Assess* 34, 1331–1351 (2020).

1098 Gaál, L. J. Szolgay, S. Kohnová, J. Parajka, R. Merz, A. Viglione, and G. Blöschl (2012),  
1099 Flood timescales: Understanding the interplay of climate and catchment processes

Formatted: Font color: Text 1

Formatted: Font color: Text 1

Formatted: Font: (Default) Arial, 12 pt, Font color: Text

Formatted: Font: (Default) Arial, Font color: Text 1

Formatted: Font color: Text 1

Formatted: Indent: Left: 0.04 cm

Formatted: Body Text, Left, Indent: Left: 0.04 cm, First line: 0 cm, Space Before: 0.65 pt, Tab stops: 2.54 cm, Left

through comparative hydrology, *Water Resour. Res.* 48, W04511, doi: Gohari, A., Shahrood, A. J., Ghadimi, S., Alborz, M., Patro, E. R., Klöve, B., & Haghighi, A. T. (2022). A century of variations in extreme flow across Finnish rivers. *Environmental Research Letters*, 17(12), 124027. DOI: 10.1088/1748-9326/aca554

Gunsolus EH, Binns AD. Effect of morphologic and hydraulic factors on hysteresis of sediment transport rates in alluvial streams. *River Res Applic.* 2018; 34: 183–192.

Gupta, H., Reddy, K.K., Gandla, V. et al. Freshwater discharge from the large and coastal peninsular rivers of India: A reassessment for sustainable water management. *Environ Sci Pollut Res* 29, 14400–14417 (2022). <https://doi.org/10.1007/s11356-021-16811-0>

Hamed, K. H., & Rao, A. R. (1998). A modified Mann-Kendall trend test for autocorrelated data. *Journal of hydrology*, 204(1-4), 182-196.

Hirvas, H., Lagerbäck, R., Mäkinen, K., Nenonen, K., Olsen, L., Rodhe, L., & Thoresen, M. (1988). The Nordkalott Project: studies of Quaternary geology in northern Fennoscandia. *Boreas*, 17(4), 431–437. <https://doi.org/10.1111/j.1502-3885.1988.tb00560.x>

Hopwood, M.J., Carroll, D., Browning, T.J. et al. Non-linear response of summertime marine productivity to increased meltwater discharge around Greenland. *Nat Commun* 9, 3256 (2018). <https://doi.org/10.1038/s41467-018-05488-8>

Hooke, J. (2003). River meander behaviour and instability: a framework for analysis. *Transactions of the Institute of British Geographers*, 28(2), 238-253.

Huo, R., Li, L., Engeland, K., Xu, C. Y., Chen, H., Paasche, Ø., & Guo, S. (2022). Changing flood dynamics in Norway since the last millennium and to the end of the 21st century. *Journal of Hydrology*, 613, 128331.

Hu, Y., Che, T., Dai, L., Zhu, Y., Xiao, L., Deng, J., & Li, X. (2023). A long-term daily gridded snow depth dataset for the Northern Hemisphere from 1980 to 2019 based on machine learning. *Big Earth Data*, 8(2), 274–301.

Huss, B., Bookhagen, C., Huggel, D., Jacobsen, R. S., Bradley, J. J., Clague, M., Vuille, W., Buytaert, D. R., Cayan, G., Greenwood, B. G., Mark, A. M., Milner, R., Weingartner, M., Winder, Toward mountains without permanent snow and ice. *Earth's Future* 5, 418–435 (2017).

Irannezhad, M., Ahmadian, S., Sadeqi, A., Minaei, M., Ahmadi, B., & Marttila, H. (2022). Peak spring flood discharge magnitude and timing in natural rivers across northern Finland: Long-term variability, trends, and links to climate teleconnections. *Water*, 14(8), 1312.

Jhajharia, D., Dinpashoh, Y., Kahya, E., Choudhary, R. R., & Singh, V. P. (2014). Trends in temperature over Godavari River basin in Southern Peninsular India. *International Journal of Climatology*, 34(5). DOI: 10.1002/joc.3761

Johansson, P. (2007). Late Weichselian deglaciation in Finnish Lapland. *Applied Quaternary research in the central part of glaciated terrain*, 47.

Kasvi, E., Alho, P., Lotsari, E., Wang, Y., Kukko, A., Hyypä, H., & Hyypä, J. (2015). Two-dimensional and three-dimensional computational models in hydrodynamic and morphodynamic reconstructions of a river bend: sensitivity and functionality. *Hydrological processes*, 29(6), 1604-1629.

Karimaei Tabarestani, M., Zarrati, A.R. Sediment transport during flood event: a review. *Int. J. Environ. Sci. Technol.* 12, 775–788 (2015).

Keciuba, W. (2021). The Role of Bedload Transport in the Development of a Proglacial River Alluvial Fan (Case Study: Scott River, Southwest Svalbard). *Hydrology*, 8(4), 173.

Korhonen, J., & Kuusisto, E. (2010). Long-term changes in the discharge regime in Finland. *Hydrology Research*, 41(3-4), 253-268.

Kunkel, K.E., Robinson, D.A., Champion, S. et al. Trends and Extremes in Northern Hemisphere Snow Characteristics. *Curr Clim Change Rep* 2, 65–73 (2016).

Formatted: English (United Kingdom)

Formatted: English (United Kingdom)

<https://doi.org/10.1007/s40641-016-0036-8>  
 Labuhn, I., Hammarlund, D., Chapron, E., Czymzik, M., Dumoulin, J. P., Nilsson, A., ... &  
 Von Grafenstein, U. (2018). Holocene hydroclimate variability in central Scandinavia  
 inferred from flood layers in contourite drift deposits in Lake Storsjön. *Quaternary*, 1(1), 2.  
 Lakens, D. (2022). Sample size justification. *Collabra: Psychology*, 8(1), 33267.  
<https://doi.org/10.1525/collabra.33267>  
 Li, C., Yang, Z., Shen, H. T., & Mou, X. (2022). Freeze-Thaw Effect on Riverbank Stability.  
*Water*, 14(16), 2479. <https://doi.org/10.3390/w14162479>  
 Li, D., Overeem, I., Kettner, A. J., Zhou, Y., & Lu, X. (2021). Air temperature regulates  
 erodible landscape, water, and sediment fluxes in the permafrost-dominated catchment on  
 the Tibetan Plateau. *Water Resources Research*, 57(2), e2020WR028193.  
 Liébault, F., Laronne, J. B., Klotz, S., & Bel, C. (2022). Seasonal bedload pulses in a small  
 alpine catchment. *Geomorphology*, 398, 108055.  
 Lintunen, K., Kasvi, E., Uvo, C. B., & Alho, P. (2024). Changes in the discharge regime of  
 Finnish rivers. *Journal of Hydrology: Regional Studies*, 53, 101749.  
 Lotsari, E., Hackney, C., Salmela, J., Kasvi, E., Kemp, J., Alho, P., and Darby, S. E.  
 (2020) Subarctic river bank dynamics and driving processes during the open-channel flow  
 period. *Earth Surf. Process. Landforms*, 45: 1198–1216. <https://doi.org/10.1002/esp.4796>.  
 Lotsari, E., Dietze, M., Kämäri, M., Alho, P., & Kasvi, E. (2020). Macro-Turbulent flow and  
 its impacts on sediment transport potential of a subarctic river during ice-covered and  
 open-channel conditions. *Water*, 12(7), 1874.  
 Lotsari, E., Vaaja, M., Flenor, C., Kaartinen, H., Kukko, A., Kasvi, E., ... & Alho, P. (2014).  
 Annual bank and point bar morphodynamics of a meandering river determined by high-  
 accuracy multitemporal laser scanning and flow data. *Water Resources Research*, 50(7),  
 5532–5559.  
 Lotsari, E., de Vet, M., Murphy, B., McLolland, S., and Parsons, D.: Defrosting river banks:  
 morphodynamics and sediment flux, EGU General Assembly 2024, Vienna, Austria, 14–  
 19 Apr 2024, EGU24-10175, <https://doi.org/10.5194/egusphere-egu24-10175>, 2024.  
 Luoto, M., Heikkinen, R.K. and Carter, T.R. (2004). Loss of palaeo-mires in Europe and  
 biological consequences. *Environmental conservation*, 31(1), pp. 30–37.  
 Doi:10.1017/s0376892904001018.  
 Malutta, S., Kobiyama, M., Borges Chaffe, P-L., Bernardi Bonumá, N; Hysteresis analysis to  
 quantify and qualify the sediment dynamics: state of the art. *Water Sci Technol* 15 June  
 2020; 81 (12): 2471–2487.. doi:  
 Mao, L. (2012). The effect of hydrographs on bed load transport and bed sediment spatial  
 arrangement, *J. Geophys. Res.* 117, F03024,. doi:10.1029/2012JF002428.  
 Mao, L. (2018). The effects of flood history on sediment transport in gravel-bed rivers.  
*Geomorphology*, 322, 196–205.  
 Matti, B., Dahlke, H., Dieppois, B., Lawler, D., & Lyon, S. (2017). Flood seasonality across  
 Scandinavia—Evidence of a shifting hydrograph? *Hydrological Processes*, 31(24), 4354–  
 4370. <http://dx.doi.org/10.1002/hyp.11365>  
 Martin, R. L. and D. J. Jerolmack (2013), Origin of hysteresis in bed form response to  
 unsteady flows, *Water Resour. Res.* 49, 1314–1333,. doi:10.1002/wrcr.20093  
 Meriö, L. J., Ala-aho, P., Linjama, J., Hjort, J., Kløve, B., & Marttila, H. (2019). Snow to  
 precipitation ratio controls catchment storage and summer flows in boreal headwater  
 catchments. *Water Resources Research*, 55(5), 4096–4109.  
 Micheletti, N., Chandler, J., & Lane, S. (2013, April). Near instantaneous production of  
 digital terrain models in the field using smartphone and Structure-from-Motion  
 photogrammetry. In EGU General Assembly Conference Abstracts (pp. EGU2013-10501).

1199 Mohammadzadeh Khani H, Kinnard C, Lévesque E. Historical Trends and Projections of  
 1200 Snow Cover over the High Arctic: A Review. *Water*. 2022; 14(4):587.  
 1201 Najafi, S., Dragevich, D., Heckmann, T., & Sadeghi, S. H. (2021). Sediment connectivity  
 1202 concepts and approaches. *Catena*, 196, 104880.  
 1203 Tananaev, N. I. Hysteresis effects of suspended sediment transport in relation to  
 1204 geomorphic conditions and dominant sediment sources in medium and large rivers of the  
 1205 Russian Arctic. *Hydrology Research* 1 April 2015; 46 (2): 232–243.. doi:  
 1206 Phillips, C. B., Hill, K. M., Paola, C., Singer, M. B., & Jerolmack, D. J. (2018). Effect of  
 1207 flood hydrograph duration, magnitude, and shape on bed load transport dynamics.  
 1208 *Geophysical Research Letters*, 45, 8264–8271.  
 1209 Pulliainen, J., Luojus, K., Derksen, C. et al. Patterns and trends of Northern Hemisphere  
 1210 snow mass from 1980 to 2018. *Nature* 581, 294–298 (2020).  
 1211 Reesink, A. J., & Bridge, J. S. (2011). Evidence of bedform superimposition and flow  
 1212 unsteadiness in unit bar deposits, South Saskatchewan River, Canada. *Journal of*  
 1213 *Sedimentary Research*, 81(11), 814–840.  
 1214 Salmela, J., Kasvi, E., Vaaja, M. T., Kaartinen, H., Kukko, A., Jaakkola, A., & Alho, P.  
 1215 (2020). Morphological changes and riffle-pool dynamics related to flow in a meandering  
 1216 river channel based on a 5-year monitoring period using close-range remote sensing.  
 1217 *Geomorphology*, 352, 106982.  
 1218 Sen, P. K. (1968). Estimates of the regression coefficient based on Kendall's tau. *Journal*  
 1219 *of the American statistical association*, 63(324), 1379–1389. DOI:  
 1220 Syvitski, J. P. (2002). Sediment discharge variability in Arctic rivers: implications for a  
 1221 warmer future. *Polar Research*, 21(2), 323–330.  
 1222 Shrestha, R. R., Bennett, K. E., Peters, D. L., Yang, D. (2021). Hydrologic Extremes in  
 1223 Arctic Rivers and Regions: Historical Variability and Future Perspectives. In: Yang, D.,  
 1224 Kane, D. L. (eds) *Arctic Hydrology, Permafrost and Ecosystems*. Springer, Cham.  
 1225 van Rooijen, E., & Lotsari, E., 2024 The spatiotemporal distribution of river bank erosion  
 1226 events and their drivers in seasonally frozen regions, *Geomorphology*, Volume 454,  
 1227 Vatne, G., Takøy Naas, Ø., Skårholen, T., Boylich, A. A., & Berthling, I. (2008). Bed load  
 1228 transport in a steep snowmelt-dominated mountain stream as inferred from impact  
 1229 sensors. *Norsk Geografisk Tidsskrift Norwegian Journal of Geography*, 62(2), 66–74.  
 1230 Veijalainen, N., Lotsari, E., Alho, P., Vehviläinen, B., & Käyhkö, J. (2010). National scale  
 1231 assessment of climate change impacts on flooding in Finland. *Journal of hydrology*, 391(3–  
 1232 4), 333–350.  
 1233 Viglione, A., Chirico, G. B., Komma, J., Woods, R., Borga, M., & Blöschl, G. (2010).  
 1234 Quantifying space-time dynamics of flood-event types. *Journal of Hydrology*, 394(1–2),  
 1235 213–229.  
 1236 Vormoor, K., Lawrence, D., Schlichting, L., Wilson, D., & Wong, W. K. (2016). Evidence for  
 1237 changes in the magnitude and frequency of observed rainfall vs. snowmelt-driven floods in  
 1238 Norway. *Journal of Hydrology*, 538, 33–48.  
 1239 Wenng, H., Barneveld, R., Bechmann, M., Marttila, H., Krogstad, T., & Skarbøvik, E.  
 1240 (2021). Sediment transport dynamics in small agricultural catchments in a cold climate: a  
 1241 case study from Norway. *Agriculture, Ecosystems & Environment*, 317, 107484.  
 1242 Williams, G. P. (1989). Sediment concentration versus water discharge during single  
 1243 hydrologic events in rivers. *Journal of Hydrology*, 111(1–4), 89–106.  
 1244 Wohl, E. (2017). Connectivity in rivers. *Progress in Physical Geography*, 41(3), 345–362.  
 1245 Zhang, T., Li, D., Kettner, A. J., Zhou, Y., & Lu, X. (2021). Constraining dynamic sediment-  
 1246 discharge relationships in cold environments: The sediment-availability-transport (SAT)  
 1247 model. *Water Resources Research*, 57(10), e2021WR030690.

Formatted: English (United Kingdom)

1248 Zhang, T., Li, D., East, A.E. et al. Warming-driven erosion and sediment transport in cold  
1249 regions. *Nat Rev Earth Environ* 3, 832–851 (2022). [https://doi.org/10.1038/s43017-022-](https://doi.org/10.1038/s43017-022-00362-0)  
1250 [00362-0](https://doi.org/10.1038/s43017-022-00362-0)  
1251 Zhang, T., Li, D., East, A. E., Kettner, A. J., Best, J., Ni, J., & Lu, X. (2023). Shifted  
1252 sediment transport regimes by climate change and amplified hydrological variability in  
1253 cryosphere-fed rivers. *Science Advances*, 9(45).